Oxygen Isotope Variability of Planktonic Foraminifera Provide Clues to Past Upper Ocean Seasonal Variability

Brett Metcalfe, Wouter Feldmeijer, Gerald Ganssen

Paleoceanography and Paleoclimatology

RESEARCH ARTICLE
10.1029/2018PA003475

Oxygen Isotope Variability of Planktonic Foraminifera Provide Clues to Past Upper Ocean Seasonal Variability

Brett Metcalfe[1,2], **Wouter Feldmeijer**[1,3], **and Gerald M. Ganssen**[1]

[1]Earth and Climate Cluster, Department of Earth Sciences, Faculty of Science, Vrije Universiteit Amsterdam, Amsterdam, The Netherlands, [2]Laboratoire des Sciences du Climat et de l'Environnement, LSCE/IPSL, CEA-CNRS-UVSQ, Université Paris-Saclay, Gif-sur-Yvette, France, [3]Now at Nebest B.V, Vianen, The Netherlands

Key Points:
- Single foraminiferal stable isotope values can provide information on the seasonality of the past
- Variance in *Globigerina bulloides* oxygen isotope values relate to insolation
- Spread in *N. pachyderma* oxygen isotope values relates to the difference between the mean value of it and its sister taxon *N. incompta*

Supporting Information:
- Supporting Information S1

Correspondence to:
B. Metcalfe,
b.metcalfe@vu.nl

Citation:
Metcalfe, B., Feldmeijer, W., & Ganssen, G. M. (2019). Oxygen isotope variability of planktonic foraminifera provide clues to past upper ocean seasonal variability. *Paleoceanography and Paleoclimatology*, *34*, 374–393. https://doi.org/10.1029/2018PA003475

Received 20 SEP 2018
Accepted 2 FEB 2019
Accepted article online 8 FEB 2019
Published online 25 MAR 2019

Abstract The major control upon abundance of planktonic foraminifera and their stable oxygen isotope ($\delta^{18}O$) signature is the seasonally linked variation in water hydrography, key to the proliferation or attenuation of ecologically beneficial constraints. The range and variance $\sigma(\delta^{18}O)$ of planktonic foraminifera can reflect changes in either the season or depth of calcification. For a detailed reconstruction of ocean changes we employed multispecies single-specimen analysis, which allows extraction of the isotopic variability within the species for the time covered by the sample. Previous studies with pooled specimens have shown that the multiannual temperature range may be extracted. Here we investigate how seasonality can be deduced from single-specimen analysis of planktonic foraminifera combined with multiple other proxies (IRD percent, faunal abundance) from Termination III. Our single-shell isotope results show that the variance in *Globigerina bulloides* oxygen isotope values corresponds to the insolation at the core site. Furthermore, faunal and isotopic analyses of the polar-subpolar neogloboquadrinid species, *N. pachyderma* (NPS) and *N. incompta*, reveal an intriguing result. These species are sister taxa, representing genetically distinct species, whose relative abundance reflects warm and cold conditions. While the difference between their isotopic means should reflect the temperature difference between their distinct growing seasons, we show that this difference also has a statistically significant relationship with the spread in individual NPS $\delta^{18}O$. At an appropriate core site, this approach could be used to further constrain the length of the growing season and therefore the inherent variability recorded within proxy records.

Plain Language Summary Reconstructions of the past climate of the Earth have focused upon the average signal, either mean annual temperature or distinct seasons (e.g., average summer or winter), as recorded by the shells of planktonic organisms in deep-sea sediments. However, these records are biased by the waxing and waning of environmental variables that benefit or hinder the growth and proliferation of individual species. The spread in isotope values recorded by individual shells can therefore give more information as to the extent of the growing period as well as provide information upon the seasonality of the past.

1. Introduction

Seasonality, the difference in a climatic variable (i.e., temperature, salinity) on an annual scale between positions in the Earth's orbit relative to the Sun, is an important regulator of both abiotic and biotic oceanic processes, with small variations having dramatic consequences. While total daily insolation plays an important role in the growth of individual phytoplankton cells through photosynthesis, the seasonal entrainment of nutrients from depth into the surface ocean through winter mixing and the subsequent warming of the water column resulting in summer stratification ensure fertile conditions for a bloom in phytoplankton communities in spring (Sverdrup, 1953; Sverdrup et al., 1942). In the northern hemisphere for instance, the annual drawdown of carbon as total organic and total inorganic carbon by the North Atlantic Ocean is 0.7 (±0.1) petagrams (Pg), yet seasonal variations in biomass and shell production lead to annual changes of ±0.3 Pg C/year (Gruber et al., 2002). Understanding whether these seasonal changes are amplified, or dampened, on longer time scales and how they interplay with various climatic boundary conditions (i.e., atmospheric pCO_2, ice sheet extent) is important for our understanding of past ocean processes. For the most part, gravitational interactions between celestial bodies alter the orbital configuration of the Earth around the Sun, leading to computable estimates of the changes in the timing, amount, and the distribution of solar

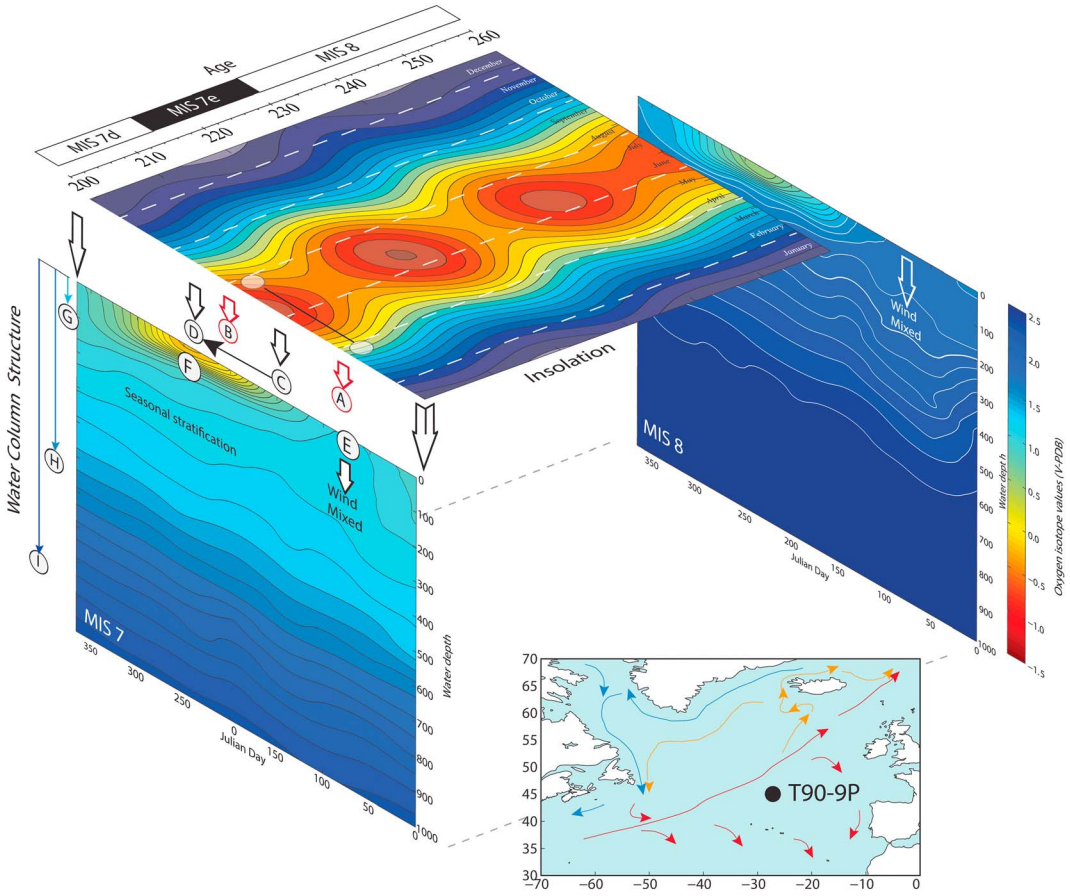

Figure 1. Schematic of the hydrography at (inset) core site T90-9P during the studied interval. Equilibrium oxygen isotope values ($\delta^{18}O_{eq}$) plotted as a function of time (Julian day) and water depth (m); indicated is the deepened wind mixed layer (e) and the later stratified water column (f). For reference the growing season of *G. bulloides* is indicated (c and d), as inferred from sediment trap data (Wolfteich, 1994) and the depth habitats of (g) *G. bulloides*, (h) *G. inflata*, and (i) *G. truncatulinoides* as established in the literature (Ganssen & Kroon, 2000; Tolderlund & Bé, 1971). Also shown is the relative monthly insolation at 45°N during the corresponding time period; note that the rise in insolation is not immediately mirrored in the water column (a and b). Insert, map of North Atlantic with location of core T90-9P indicated (Metcalfe et al., 2015). Arrows represent the location and direction of surface water masses, and the color represents the relative temperature from warm (red) to cold (blue).

radiation (insolation) at the top of the atmosphere through time. Three dominant orbital parameters that force the climate system are used by paleoclimatologists to best describe the changes in orbital configuration: the shape of the Earth's orbit around the Sun (eccentricity), the distance between the Sun and the Earth at the summer solstice (precession), and the tilt of the Earth's axis (obliquity; Figure 1). Of these, the total annual mean insolation is altered only by changes in eccentricity, whereas changes in both precession and eccentricity alter the length of seasons, from a minimum length of 82.5 days to a maximum of 100 days (the present-day length of the seasons varies being between 89 and 92 days). In contrast, changes in obliquity alter the distribution of heat between low and high latitudes.

1.1. Aims and Objectives

Although orbital parameters can be computed (Figure 1 and Figure S1 in the supporting information), the quantification of the effect of changes in past seasonality from the geological record has predominately focused on annually layered sediments (varves), regions of unprecedented high sedimentation (i.e., drift deposits), and/or biomineralizers that produce (sub) annual layers. This approach excludes much of the open ocean, in which the sedimentation rate is far less (Lougheed et al., 2018; Olson et al., 2016), while placing a far greater emphasis on reconstructions from shallow marine and continental shelf settings. Techniques aiming to disentangle past changes in seasonality have considered both the interspecies distribution of the stable oxygen isotope ($\delta^{18}O$) composition of planktonic foraminifera (Ganssen &

Kroon, 2000) and the intraspecies variability in single shells of foraminifera, or $\sigma(\delta^{18}O)$ (Koutavas et al., 2006; Koutavas & Joanides, 2012; Leduc et al., 2009; Scussolini et al., 2013; Wit et al., 2010). Emiliani (1954), for instance, showed early on that not only do foraminifera have distinct depth habitats and ecological niches but that their shells are capable of recording past upper ocean variability. Further noting at the time that while single foraminiferal analysis was unattainable at the time, it would provide an opportunity to expand the ecological information of the individuals within the population (Emiliani, 1954). Likewise, Mix (1987) proposed that the temperature recorded in the mean isotopic composition is weighted toward the season that overlaps the species temperature tolerance (Jonkers & Kucera, 2017; Mulitza et al., 1998; Roche et al., 2018). Through comparison between species with different ecologies, that is, warm and cold-water species, and depth habitats, that is, surface and thermocline dwelling species, a measure of the temperature distribution, both seasonally and vertically can be obtained (Ganssen et al., 2011; Wefer et al., 1996).

Recently, we conducted single-specimen analysis (or individual specimen analysis) on T-III of the lower section of piston core JGOFS-T90-9p (45°17.5′N, 27°41.3′W; water depth 2934 m) with the intention to unravel size-isotope artifacts in oxygen ($\delta^{18}O$) and carbon ($\delta^{13}C$) isotope measurements of three planktonic foraminiferal (morpho)species (Figure 2), *Globigerina bulloides*, *Globorotalia inflata*, and *Globorotalia truncatulinoides* (dextral and sinistral; Feldmeijer et al., 2015; Metcalfe et al., 2015). Glacial terminations, an abrupt transition from Glacial to Interglacial climate, represent an intriguing period of study as they capture several oceanic modes over a relatively short period of time (Denton et al., 2010). Evidence of the role of seasonality on abrupt climate change at the last Termination (Denton et al., 2005, 2010) has shown that it acts as an amplifier of extreme conditions (Chiang & Bitz, 2005; Isarin et al., 1998; Isarin & Renssen, 1999; Isarin et al., 1999; Renssen & Isarin, 2001). Yet while several Glacial Terminations have been identified as analogous, in terms of equivalent orbital parameters, with the most recent Termination I (T-I), there are others that have different orbital and boundary conditions. Investigation of such Terminations, with different orbital parameters, is critical for understanding what the common similarities are and which processes can be considered event specific (Pérez-Mejías et al., 2017). The Glacial termination between Marine Isotope Stages 8 and 7, Termination III (T-III), occurs at a time of dissimilar orbital conditions from those of T-I with an ~10-kyr lag between maximum obliquity and minimum precession. Of the Terminations of the past ~450 kyr it is one that is distinctly muted (Cheng et al., 2009), being referred to as a "low-amplitude" termination (Lang & Wolff, 2011) that gives rise to the weak Interglacial MIS 7 that rapidly plunges back into Glacial conditions (Lang & Wolff, 2011; Pérez-Mejías et al., 2017). Such an interruption of interglacial conditions makes it similar to T-I, which is a Termination interrupted by stadial conditions, despite having dissimilar orbital parameters making it an interesting objective for paleoclimate research (Pérez-Mejías et al., 2017). Further similarities include the ice-rafting events during Glacial MIS 8 having detrital carbonate that has similar provenance, the Hudson Strait, as the Heinrich events of the last glacial unlike MIS 6 (Obrochta et al., 2014). The aim of this paper is to investigate the range and variability in the $\delta^{18}O$ composition of several species of foraminifera to interpret changes during T-III and over MIS 8 and 7, using a multispecies approach in combination with faunal abundance counts. In the course of doing this, we have discerned a relationship between the $\sigma(\delta^{18}O)$ of the polar species *Neogloboquadrina pachyderma* and the isotopic difference ($\Delta\delta^{18}O$) from its sister taxa *Neogloboquadrina incompta* that represents more subpolar to temperate climatic conditions; we herein describe and interpret these results.

2. Analytical Methodology

2.1. Samples: Piston Core T90-9P

Between 728- and 828-cm core T90-9p was sliced into 1-cm samples at ~4-cm intervals; this section of T90-9P (Feldmeijer et al., 2015; Lototskaya et al., 1998; Lototskaya & Ganssen, 1999; Metcalfe et al., 2015; van Kreveld et al., 1996) covers the transition from MIS 8 and MIS 7 (Figures 1 and 3). The age depth relationship (Table 1) is that of Feldmeijer et al. (2015), with the downcore record of *G. inflata* tuned to the "planktonic foraminifera" depth-derived $\delta^{18}O$ stack of Huybers (Huybers, 2007) to both avoid circular reasoning and preclude the evaluation of orbital parameters (Huybers, 2007; Huybers & Wunsch, 2004).

Faunal and terrigenous (i.e., IRD) counts were made on a split of ~250 specimens per each size fraction (212–250, 250–300, 300–355, and 355–400 μm) from each sample and converted into numbers per gram

10.1029/2018PA003475

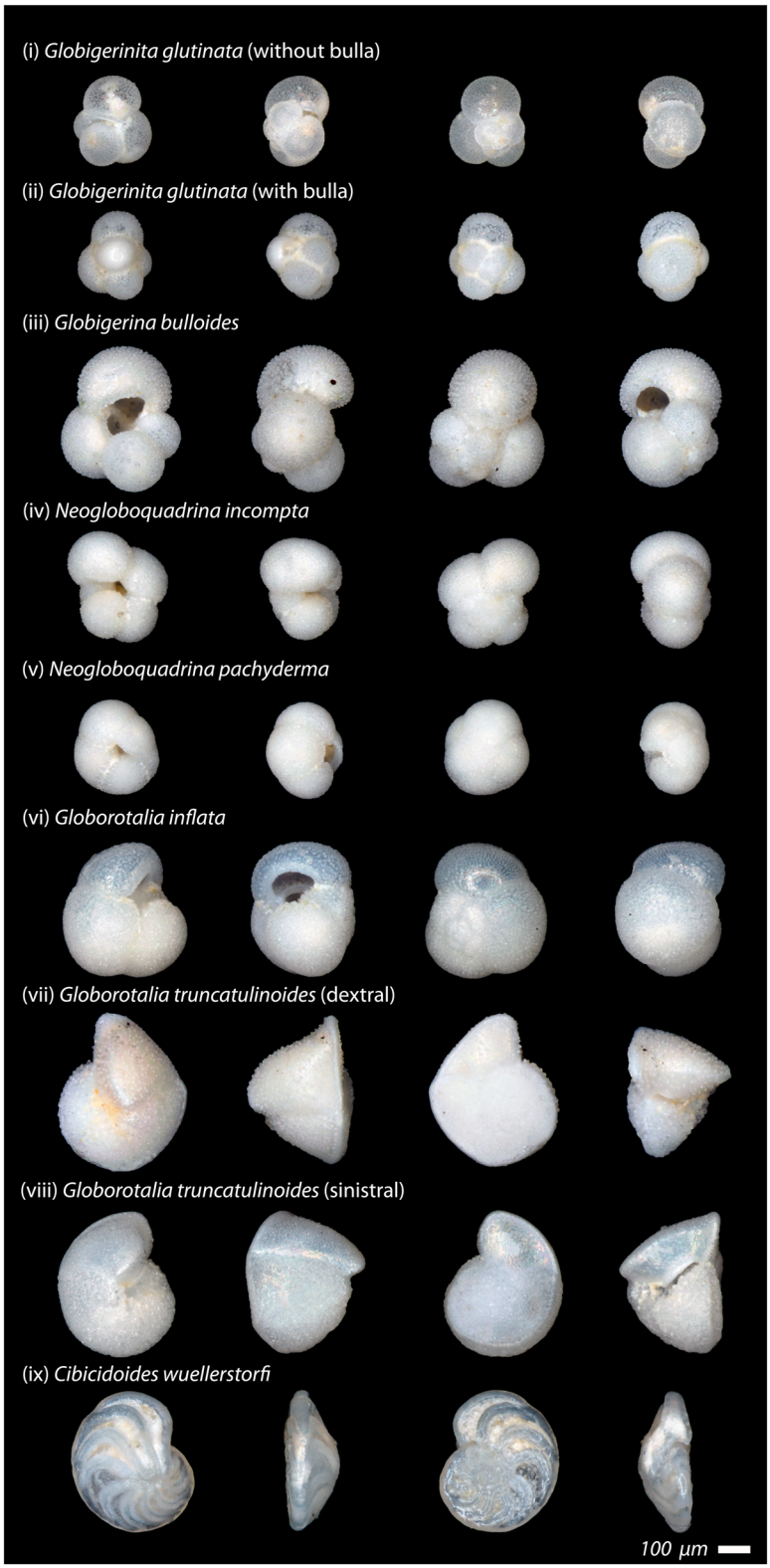

Figure 2. Taxonomy of termination III (T-III) in piston core JGOFS T90-9p. Species measured for stable isotopes from T-III in aperture, side, spiral, and side views: (i and ii) *Globigerinita glutinata*, (iii) *Globigerina bulloides*, (iv) *Neogloboquadrina incompta*, (v) *Neogloboquadrina pachyderma*, (vi) *Globorotalia inflata*, (vii and viii) *Globorotalia truncatulinoides*, (vii) dextral and (viii) sinistral, and the benthic foraminifera (ix) *Cibicidoides wuellerstorfi*. Scale bar is 100 μm for all pictured foraminifera.

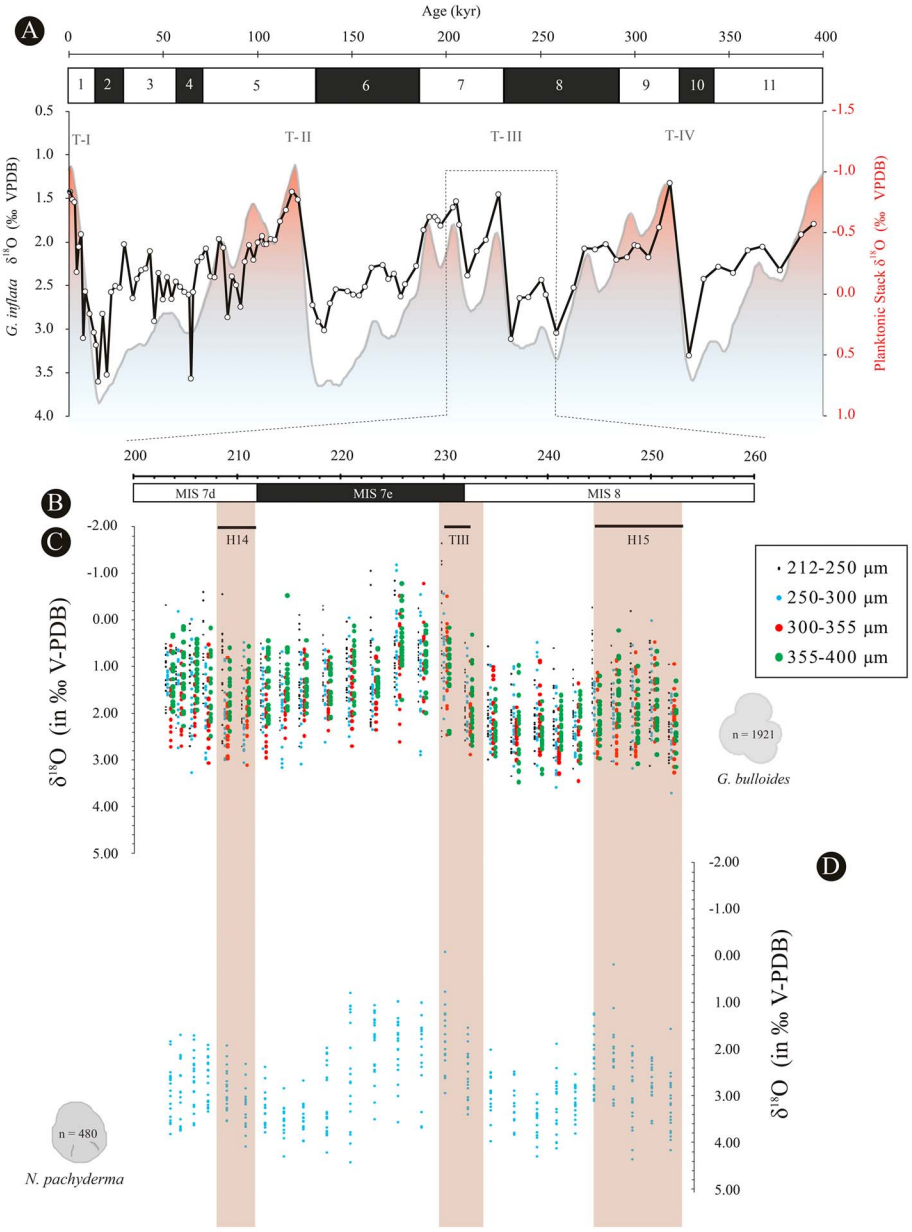

Figure 3. Raw single-specimen oxygen isotope values. (a) Age versus oxygen isotope ($\delta^{18}O$) values of *Globorotalia inflata* (Feldmeijer et al., 2015; Metcalfe et al., 2015) with the record selected as a tuning target, the planktonic stack of Huybers (2007), plotted alongside. (b) Marine isotope stages (MIS) of the core interval analyzed for single specimens of (c) *G. bulloides* (Metcalfe et al., 2015) and (d) *N. pachyderma* (this paper).

using the sample dry weight. For single-shell analysis, two surface dwelling species, *G. bulloides* and *N. pachyderma* (sinistral/left-coiling also referred to as NPS), and two deeper dwellers, *G. inflata* and *G. truncatulinoides*, were picked out from narrow size fractions to exclude potential vertical migration during ontogeny (250–300 µm for *N. pachyderma* and 300–355 µm for others). Single-specimen data of *G. bulloides*, *G. inflata*, and *G. truncatulinoides* (sinistral and dextral coiling direction) from the 300–355 µm have been published previously (Feldmeijer et al., 2015; Metcalfe et al., 2015). In conjunction with these previous measurements, 20 individuals of *N. pachyderma* from the 250–300 µm were picked from each sample, weighed in groups of 5 using a Sartorius Microbalance, measured for size using a Nikon digital research microscope, and analyzed singularly for stable isotopes. Pooled specimens of the surface-dwelling planktonic foraminifera *G. glutinata* and *N. incompta* (2 measurements of a group of 10

Paleoceanography and Paleoclimatology

10.1029/2018PA003475

Table 1
Proxy Data Generated Through Micropaleontological and Geochemical Analyses Against Depth and Age

	Abundance Counts					Oxygen Isotopes ($\delta^{18}O$)					Difference in Oxygen Isotope Values ($\Delta\delta^{18}O$)				
Depth in Core (cm)	Percent Abundance *G. bulloides* (in %)	Percent Abundance *G. inflata* (in %)	Percent Abundance *G. truncatulinoides* (in %)	Percent Abundance *G. ruber* (in %)	Coiling Ratio of Neogloboquanids (% *N. incompta*)	*C. wuellerstorfi* ($\delta^{18}O$ in ‰ V-PDB)	*G. glutinata* ($\delta^{18}O$ in ‰ V-PDB)	*N. pachyderma* ($\delta^{18}O$ in ‰ V-PDB)	*N. incompta* ($\delta^{18}O$ in ‰ V-PDB)	*N. pachyderma* Standard Deviation ($\delta^{18}O$ in ‰ V-PDB)	Benthic Versus *N. pachyderma* ($\Delta\delta^{18}O$ in ‰ V-PDB)	Benthic-Planktonic ($\Delta\delta^{18}O$ in ‰ V-PDB)	*N. pachyderma*-*N. incompta* ($\delta^{18}O$ in ‰ V-PDB)	Temperature Difference (*G. bulloides* Versus *G. inflata*)	Age
729	24.56	29.39	1.75	2.30	77	2.46	0.84	2.70	1.36	0.57	−0.24	1.61	1.33	1.72	203.4
732	22.60	27.26	2.70	1.82	80	2.99	1.36	2.72	1.65	0.66	0.27	1.63	1.07	1.20	204.4
736	26.96	27.04	1.73	1.03	60	3.01	1.22	2.85	1.50	0.55	0.17	1.79	1.35	1.11	205.7
740	26.10	29.95	2.63	1.10	52	2.93	1.11	2.63	1.57	0.48	0.31	1.82	1.06	0.17	207.0
744	31.72	18.51	1.38	0.94	41	3.48	1.22	3.18	1.95	0.44	0.30	2.26	1.23	0.93	208.9
748	27.42	20.56	1.76	0.36	72	3.71	1.56	3.69	1.64	0.44	0.02	2.15	2.05	1.77	210.7
752	24.63	29.62	5.16	0.75	89	3.78	1.30	3.39	2.00	0.37	0.40	2.49	1.39	2.44	212.6
756	22.04	30.18	7.21	0.56	85	3.36	1.37	3.26	1.81	0.32	0.10	1.99	1.45	1.97	214.5
760	18.88	30.83	5.02	0.17	93	3.18	1.09	3.31	1.68	0.32	−0.13	2.09	1.63	2.33	216.3
764	16.40	32.40	4.94	0.93	99	3.24	1.43	2.30	1.74	0.71	0.94	1.81	0.56	3.35	218.6
768	20.67	35.79	4.79	0.65	99	2.61	1.51	1.89	1.61	1.16	0.72	1.10	0.28	3.13	220.9
772	16.61	38.09	5.00	1.70	95	3.08	1.24	1.87	1.59	0.71	1.21	1.84	0.28	2.73	223.2
776	18.78	37.82	4.83	3.17	78	2.79	0.92	2.10	1.24	0.64	0.69	1.87	0.86	3.95	225.5
780	28.47	26.94	2.67	3.73	64	2.39	1.04	1.64	1.08	0.84	0.75	1.35	0.56	3.30	227.8
784	31.51	14.64	1.97	2.41	35	3.00	0.71	1.42	1.48	0.74	1.58	2.29	−0.06	3.76	230.1
788	24.27	5.70	0.51	0.50	13	3.35	2.25	2.61	2.04	0.56	0.74	1.10	0.56	0.80	232.3
792	29.65	6.67	0.88	0.75	28	3.61	2.40	2.78	1.96	0.47	0.83	1.21	0.82	0.33	234.6
796	26.82	8.07	0.99	0.51	42	3.68	1.60	3.48	2.46	0.46	0.21	2.08	1.01	0.99	236.8
800	21.33	10.18	0.81	0.54	68	3.85	1.93	3.54	2.15	0.33	0.31	1.92	1.39	0.35	239.1
804	22.57	10.69	0.47	0.44	79	4.01	2.28	3.52	2.40	0.60	0.49	1.73	1.13	0.08	240.9
808	22.08	14.05	1.73	0.32	86	3.94	1.90	2.96	1.91	0.35	0.98	2.04	1.05	0.03	242.8
812	20.76	14.99	1.17	0.63	87	3.83	1.94	2.77	2.12	0.59	1.06	1.89	0.65	2.33	244.6
816	17.47	10.44	2.57	1.39	73	3.62	2.03	2.07	1.97	0.74	1.54	1.59	0.10	1.40	246.5
820	24.10	16.62	0.55	0.28	82	-	1.84	2.83	2.21	0.73	-	-	0.62	0.41	248.4
824	21.23	17.32	2.11	0.68	88	3.60	1.85	3.20	2.05	0.41	0.40	1.76	1.16	2.01	250.2
828	12.46	11.28	0.37	0.67	90	3.36	1.63	3.59	2.19	0.62	−0.22	1.73	1.40	0.65	252.1

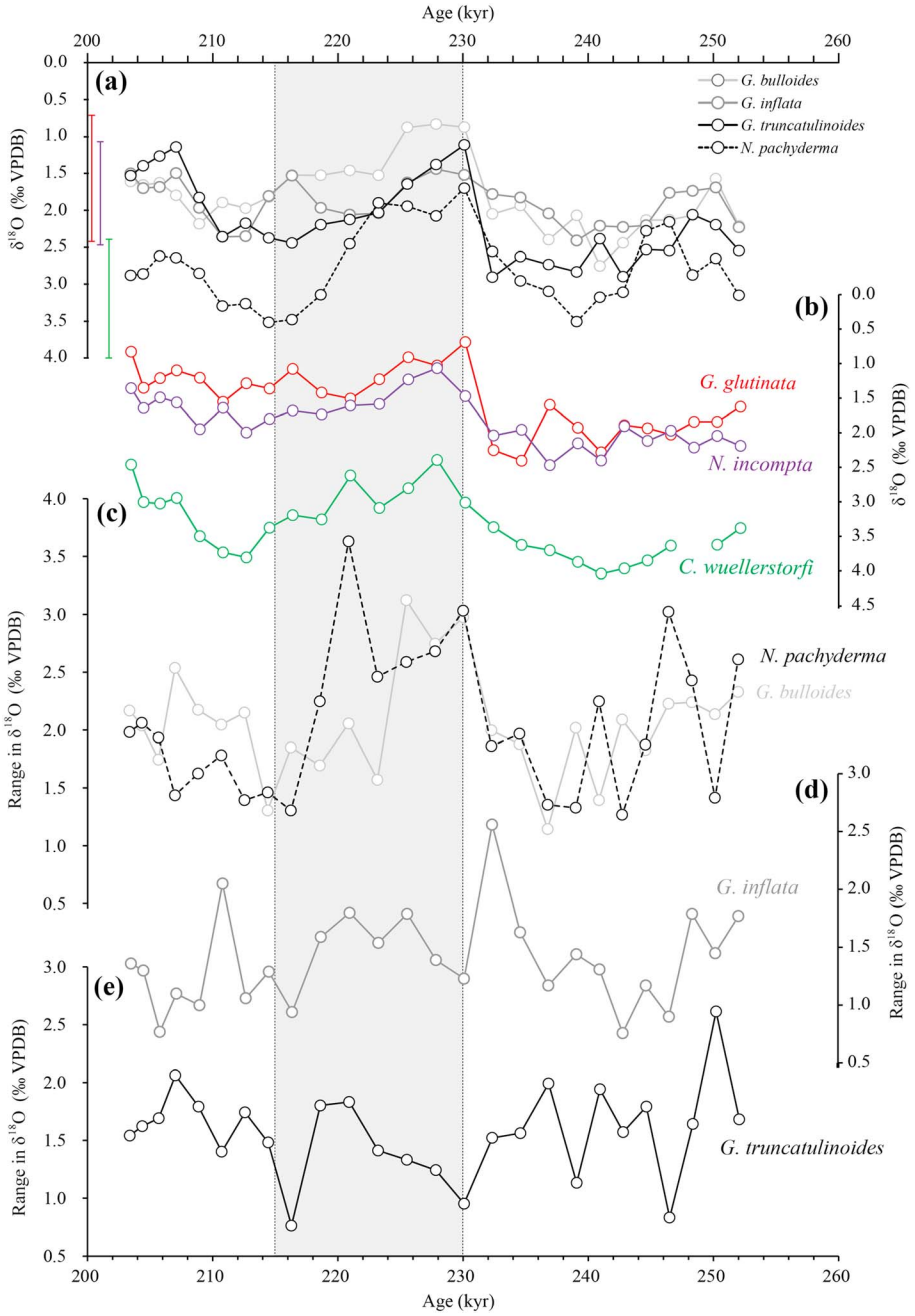

Figure 4. Mean and standard deviation of measured planktonic foraminifera from T-III. (a) Mean planktonic oxygen isotope curves for *G. bulloides*, *N. pachyderma*, *G. inflata*, and *G. truncatulinoides*. The $\delta^{18}O$ records are based on analysis of 20 single shells for the 300–355-μm size fraction for *G. bulloides*, *G. inflata*, and *G. truncatulinoides* and 20 single shells for 250–300 μm of *N. pachyderma*. (b) Bulk planktonic oxygen isotope curves for *G. glutinata* and *N. incompta* and benthic curve for *C. wuellerstorfi*. Stable oxygen isotope ranges for (c) *G. bulloides* and *N. pachyderma* and (d) *G. inflata* and *G. truncatulinoides*.

specimens) as well as the benthic foraminifer *C. wuellerstorfi* (a single measurement of a group of between 2 and 10 specimens) were measured for stable isotopes (Figures 2–4 and Table 1).

Detecting temperature changes from the oxygen isotope ratio of foraminiferal shells alone is not possible as it is a product of the ambient oxygen isotope seawater ($\delta^{18}O_{sw}$), an artifact of both ice volume and water mass provenance, and the ambient temperature during growth. The change in the ratio/proportion

between *N. pachyderma* and the dextral form *N. incompta* provides an additional tool (Darling et al., 2006), as the presence of *N. pachyderma* has been identified as an indicator for the invasion of polar water at the core location (Penaud et al., 2008). For this analysis the first hundred specimens of either *N. pachyderma* or *N. incompta* were counted for each sample from the 250–300-μm size fraction and the resultant ratio computed (Table 1).

2.2. Shell Geochemistry ($\delta^{18}O$) and ($\delta^{13}C$)

Oxygen ($\delta^{18}O$) and carbon ($\delta^{13}C$) isotope measurements were performed at the VU University Amsterdam using a Thermo Finnigan Delta^{+} Mass spectrometer with a coupled GasBench II preparation device. Samples are placed in 3-mL exetainer vials with a few glass beads and sealed with a cap with a pierceable septum. The ambient air was evacuated and replaced with helium; this helium is used as a carrier gas for the CO_2 released from the carbonate shells when phosphoric acid (H_3PO_4) is added to the sample at a constant temperature of 45 °C. The glass beads ensure that there is contact between the foraminifer and the acid (Feldmeijer et al., 2015; Lougheed et al., 2018; Metcalfe et al., 2015; Pracht et al., 2018), while also helping to regulate the temperature of the reaction itself important for fractionation/partitioning of oxygen between the resulting water and carbon dioxide ($2H_3PO_{4\ (aq)} + 3CaCO_{3\ (s)} = Ca_3(PO_4)_{2\ (aq)} + 3CO_{2\ (g)} + 3H_2O_{\ (aq)}$). Between the addition of phosphoric acid and subsequent analysis of the gas 160-min elapse, this is to ensure that the sample is completely digested by the acid. The He-CO_2 is transported to the GasBench II using a flow-through system where the mixture is "cleaned" and "purified" first using Nafion tubing to remove water and then a gas chromatography column to separate other gases. The purified CO_2 is then analyzed in the mass spectrometer. Isotope values are reported following the standard δ notation in per mil (‰) versus Vienna Peedee Belemnite. In-run standards of NBS-19, IAEA-CO1, and VICS (the VU Internal Carbonate Standard) are separately used to produce a CO_2-gas amplitude (in mV) calibration curve and to check the reproducibility of each run. Reproducibility of in-run analyzed laboratory standards is less than <0.12‰ (1σ) for both $\delta^{18}O$ and $\delta^{13}C$ of small sample measurements (>5 μg). During analysis of groups of foraminifera, in which sample weight is considerably larger (60–150 μg), the reproducibility of the same laboratory standards is considerably better (1σ <0.10‰) due to a reduction in the influence of heterogeneities present within the standard (Ishimura et al., 2008).

3. Results

3.1. Oxygen Isotope Values

The raw single-shell data (Feldmeijer et al., 2015; Metcalfe et al., 2015), including the new single-shell measurements of *N. pachyderma*, are presented in Figure 3; the computed mean and range in $\delta^{18}O$ for the seven analyzed planktonic species and one epibenthic species are shown in Figure 4, for the core interval representing 200 to 260 ka. The absolute values, ignoring potential vital effects, of *G. bulloides*, *G. inflata*, and *G. truncatulinoides*, are similar to those of *N. incompta* and *G. glutinata* while *N. pachyderma* has similar values to the benthic species *C. wuellerstorfi* (vertical bars in Figure 4a). In general, most species start to show a decrease in values of $\delta^{18}O$ around 240 ka, 10 kyr prior to the Termination; following the Termination an increase in values of $\delta^{18}O$ occurs before another decrease occurs at 210 ka. The precise timing and effect of the Termination varies between species, with the Termination being more pronounced in $\delta^{18}O$ values of *G. glutinata*, *G. truncatulinoides*, and *G. bulloides*, whereas both *G. inflata* and *N. incompta* give a more muted signal. While having similar values of $\delta^{18}O$ the benthic signal records an earlier onset of Termination III (~241 ka) than *N. pachyderma*, the planktonic signal lagging the benthic signal by approximately ~2 kyr. Most notably the range in $\delta^{18}O$ of *G. bulloides* and *N. pachyderma* increases toward the deglaciation (Figure 4c); the deeper living species *G. inflata* and *G. truncatulinoides* (Figures 4d and 4e), however, reveal no clear trend in range in $\delta^{18}O$ apart from a drop at Termination III and a slow increase during MIS7e.

Surface dwelling *N. pachyderma* shows a peak in $\delta^{18}O$ range (~3.0‰) at ~246 ka (Figure 4c) caused by individuals with more depleted $\delta^{18}O$ values attributed to isotopically light meltwater during Heinrich event (HE) 15. *Globigerina bulloides* (Figure 4c), *G. inflata* (Figure 4d), and *G. truncatulinoides* (Figure 4e) seem unaffected by this meltwater signal, potentially because of either a reduction in ecological space during ice rafting and/or a relatively deeper depth habitat that is unaffected by the freshwater lid. The range in

$\delta^{18}O$ of *G. bulloides* and *N. pachyderma* increases toward the transition from glacial to MIS7e (Figure 4c), implying an increase in seasonal variability in sea surface temperature (SST) but also large amounts of freshwater influx affecting these surface dwellers. This range decreases again toward the presumably colder interglacial substage MIS7d. Furthermore, the deeper living species *G. inflata* and *G. truncatulinoides* reveal no clear trend in range in $\delta^{18}O$ apart from a drop at Termination III and a slow increase during MIS7e as to be expected with the low-temperature/salinity variability within their depth habitat (Figure 1).

3.2. Additional Proxies

There are three pronounced peaks in IRD: the two occurring at ~250 and ~210 ka are tentatively assigned as Heinrich events (HE) and the third at ~230 ka is likely a Termination Ice Rafting Event (Venz et al., 1999) associated with ice sheet decay at Termination III. The abundance of *Globigerinoides ruber* (0 to 4%; Figure 5k) peaks several samples after the increase in IRD; the variation in abundance of this warm species lags *G. bulloides* (10 to 35%; Figure 5l), a species with an affinity for colder water. The peak in the cold species occurs prior to the termination.

While the $\delta^{18}O$ of *N. pachyderma* follows a similar pattern with *C. wuellerstorfi* $\delta^{18}O$, indicative of the global ice volume effect, our results downcore also show that the coiling ratio *N. pachyderma* $\delta^{18}O$ are not in alignment (Figures 5a and 5b). The spread in single-shell *N. pachyderma* $\sigma(\delta^{18}O)$ lies between 0.2 and 1.2‰ (Figure 5c); for the same sections the $\Delta\delta^{18}O$ between *N. pachyderma* and *N. incompta* is between 0 and 2‰ (Figure 5d). Intriguingly, comparison between these two parameters, the $\Delta\delta^{18}O$ and $\sigma(\delta^{18}O_{NPS})$, reveals a correlation with larger $\Delta\delta^{18}O$ correlating with smaller $\sigma(\delta^{18}O_{NPS}$; Figure 6). While neither the $\Delta\delta^{18}O$ nor the $\sigma(\delta^{18}O)$ of *N. pachyderma* correlates with insolation, this may reflect the position of the core site with respect to *N. pachyderma*'s southerly biogeographic limit during the interglacial. The poleward shift of the polar front from its Glacial to its Interglacial position would have led to a considerable reduction in the biogeography, given the species affinity with polar waters. Comparison of *G. bulloides* $\sigma(\delta^{18}O)$, a species that exists at the core site throughout Glacial and Interglacial conditions, shows that a correlation exists between *G. bulloides* $\sigma(\delta^{18}O)$ and insolation (Figures 5f and 5g).

4. Discussion

4.1. MIS 8, MIS 7, and Termination III

The benthic $\delta^{18}O$ signal, as well as that of *N. pachyderma*, shows a relatively early onset of the glacial–interglacial termination as opposed to the shifts seen in the $\delta^{18}O$ records of *G. bulloides*, *G. glutinata*, *G. inflata*, *G. truncatulinoides*, and *N. incompta* (Figures 3 and 4). The gradual depletion of the benthic signal may reflect changes in ice volume, and/or $\delta^{18}O_{sw}$ through water mass reorganization, rather than temperature variability due to the minor influence of this variable at the core depth (2,934 m). The early onset of Termination III in the benthic signal (~241 ka) does not fit with this pattern, and could suggest a potential warming of bottom waters due to the reinstatement of circulation inducing calving of the glacial ice sheet. *N. pachyderma*, a polar species living during the coldest part of the year, lags the benthic depletion in $\delta^{18}O$ by ~2 kyr. The lag could imply that the winters began to warm up prior to the other seasons due to the effect of the Termination. This lag may in fact be less, as it is dependent upon the sampling frequency of core T90-9P in both the time and depth domain (Pisias & Mix, 1988; Wunsch, 2000; Wunsch & Gunn, 2003). The other planktonic species (i.e., *G. bulloides*, *G. glutinata*, *G. inflata*, *G. truncatulinoides*, and *N. incompta*) show a very mild, gradual depletion lagging *N. pachyderma* by ~2 kyr.

The return to interglacial $\delta^{18}O$ values at ~230 ka within ~2 kyr suggests that the final stage of Termination III is very rapid and the seasonal hydrological buildup of the water column is restored in a relatively brief period. During MIS 7e there is a differentiation between species living at the surface and intermediate-deep dwellers, again, likely a result of the reconfiguration of the various North Atlantic water masses and the retreat of the polar front. *N. pachyderma* continues to remain more enriched than the other planktonic species at the onset of MIS 7e; however, this offset when considered in relation to deep-dwelling foraminiferal oxygen isotope values decreases, before later increasing to become more enriched close to the onset of MIS 7d. The other planktonic foraminiferal species decrease in mean $\delta^{18}O$ during the lower part of MIS 7e, however not at the same magnitude as *N. pachyderma*. Benthic $\delta^{18}O$ closely follows the *N. pachyderma* curve albeit with a lag of 2 kyr, suggesting a sluggish poorly ventilated deep ocean not so dissimilar to

10.1029/2018PA003475

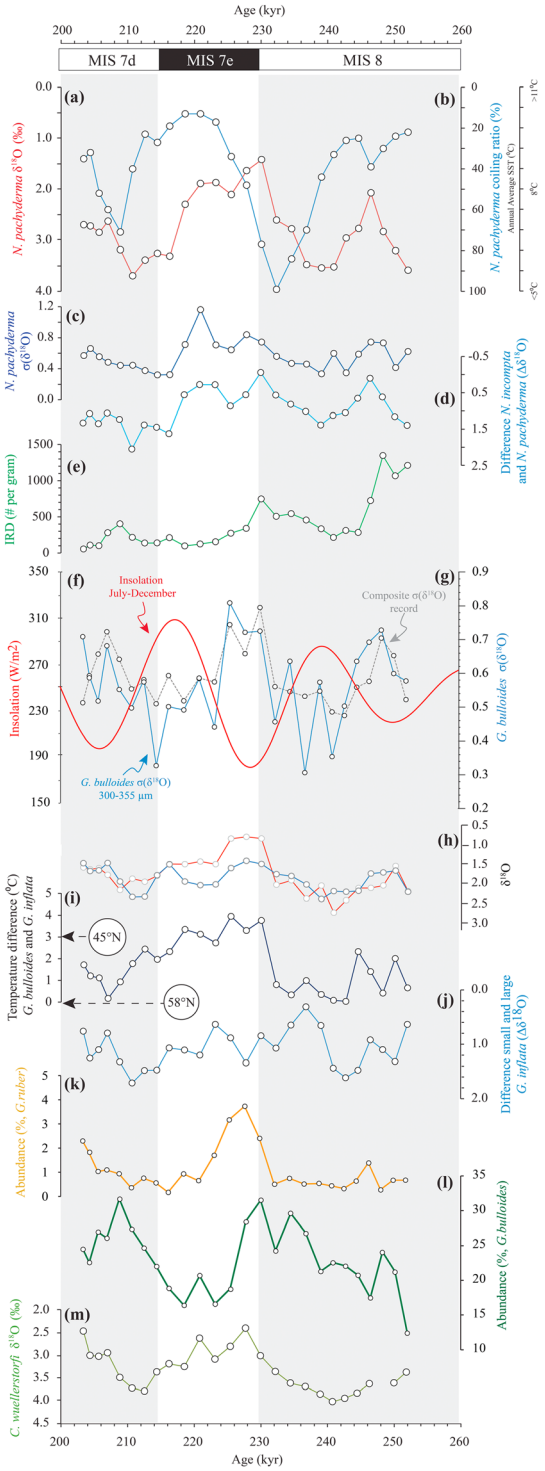

Figure 5. Downcore proxies for T-III. (a) Oxygen isotope of *N. pachyderma* plotted alongside (b) the coiling ratio of *N. pachyderma* versus *N. incompta* (in % *N. pachyderma*) with an addition temperature axis as derived from Darling et al. (2006). (c) The standard deviation of *N. pachyderma* and the (d) $\Delta\delta^{18}O$ between *N. pachyderma* and *N. incompta*. (e) IRD abundance. (f) Insolation change at 45°N. (g) Individual size fraction (300–355 μm) in blue and composite in gray $\sigma(\delta^{18}O)$ of *G. bulloides*. (h) Oxygen isotope values of *G. bulloides* and *G. inflata*. (i) Stratification index as per the study of Ganssen and Kroon (2000), that is, $\delta^{18}O$ of *G. bulloides* minus $\delta^{18}O$ of *G. inflata* converted to temperature using a linear approximation of −0.22‰ per degree Celsius for the equation of Kim & O'Neil (1997). (j) $\Delta\delta^{18}O$ between large (>250 μm) and small (212–250 μm) *G. inflata*. (k) Abundance of *Globigerinoides ruber*. (l) Abundance of *G. bulloides*. (m) Benthic oxygen isotope curve for *C. wuellerstorfi*. MIS = marine isotope stages.

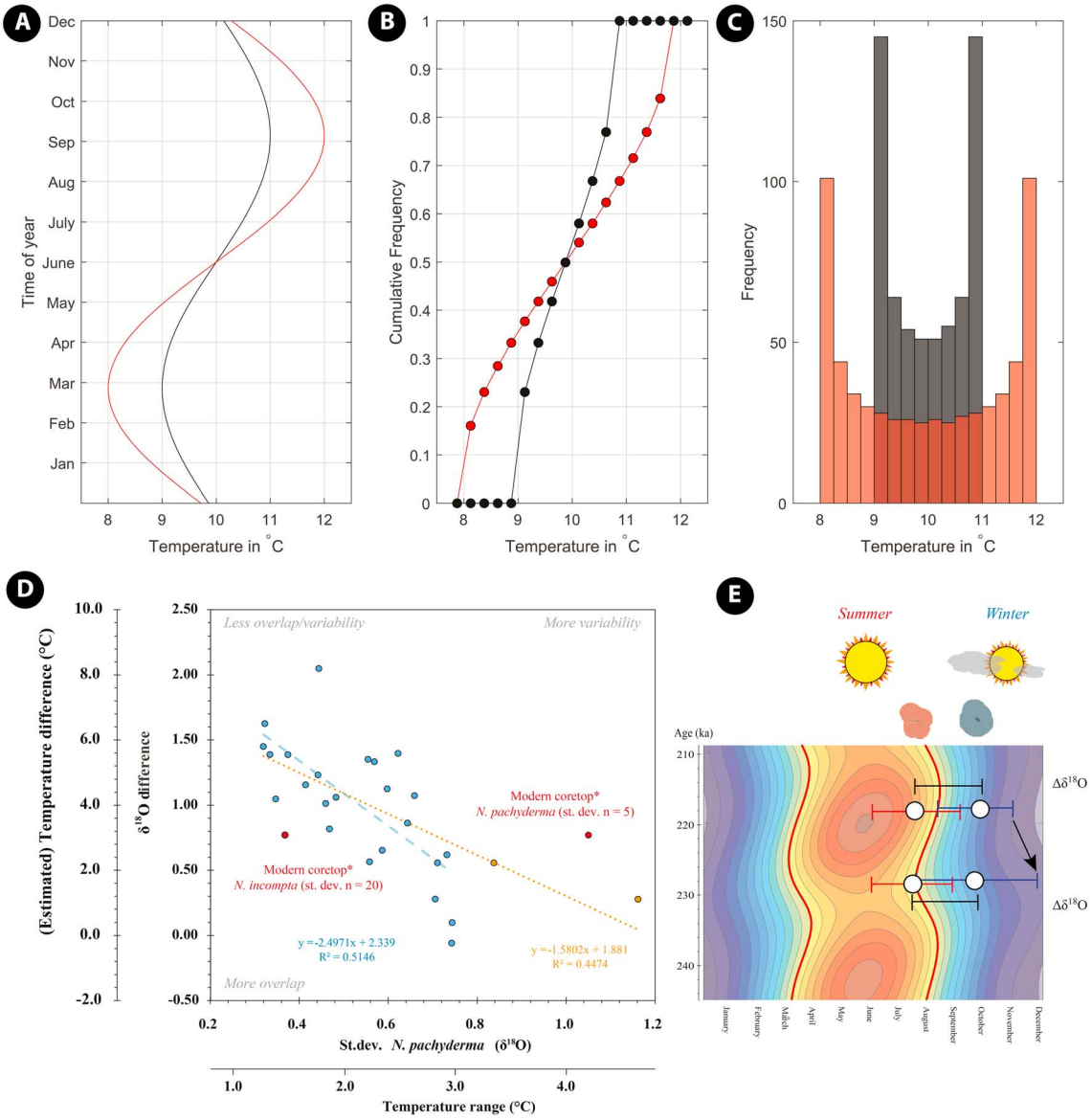

Figure 6. Comparison between temperature distributions and the isotopes of *Neogloboquadrina pachyderma* and *Neogloboquadrina incompta*. (a) Two sine waves are used as models of the time of the year against the temperature; these high (red) and low (black) amplitude distributions are plotted as (b) a cumulative frequency distribution and (c) a histogram against temperature. (d) The difference between *N. pachyderma* and *N. incompta* mean oxygen isotope values ($\Delta\delta^{18}O$) versus the standard deviation of the single-shell analysis ($\sigma(\delta^{18}O)$) of *N. pachyderma*. (e) Schematic showing the variability in *N. pachyderma* and *N. incompta* in comparison with the change in insolation. Estimate temperature difference based upon the 0.2‰ per °C (Kim & O'Neil, 1997).

glacial conditions. The transition into substage MIS7d represents a return to colder conditions as one of the two (MIS7b) relatively brief colder stages during MIS7 (Lang & Wolff, 2011). Mean $\delta^{18}O$ values of *G. bulloides*, *G. glutinata*, *G. inflata*, *G. truncatulinoides*, and *N. incompta* show a (slight) enrichment in $\delta^{18}O$ after the onset of this drop during MIS7e, with *Cibicidoides wuellerstorfi* returning to glacial $\delta^{18}O$ values (Figure 4b).

To understand the implications of our new IRD data (Figure 5e), tentatively suggested to be Heinrich events (HE; Obrochta et al., 2014) 14 (~210 kyr), HE 15 (~249 kyr; Figure 3b), and a Termination Ice Rafting Event, upon the structure of the water column a stratification index was applied to our previously published *G. bulloides* and *G. inflata* data (Metcalfe et al., 2015). The difference ($\Delta\delta^{18}O$) between the $\delta^{18}O$ of species with "known" depth habitats corresponding with shallow and deep has been used as a stratification proxy (Ganssen & Kroon, 2000; Lototskaya & Ganssen, 1999; Mulitza et al., 1997) that can be converted into an

approximate temperature difference by considering that a change of −0.22‰ occurs per °C increase, following the equation of Kim and O'Neil (1997). For the North Atlantic Ocean, Ganssen and Kroon (2000) used *G. bulloides* that dwells at a shallower depth then *G. inflata*, and considered that when $\Delta\delta^{18}O$ equals (or approaches) zero, such as for example occurring in the modern ocean at approximately 58°N, then the water column is considered to have mixed down to the permanent thermocline, while higher values indicate a stratified water column. Applying this stratification indicates that conditions during MIS 7 were similar to the present interglacial, while during MIS 8 the ocean at our core site was predominately well mixed (Figure 5i). During a peak in mixing between 242 and 232 kyr, the abundance of *G. bulloides* and IRD as well as the standard deviation of *N. pachyderma* increases, which could point toward an elevated influx of freshwater.

Metcalfe et al. (2015) further examined this freshwater input through the calculation of the difference between the $\delta^{18}O$ of different sized *G. inflata* (212–250 μm and >250 μm) shells (Figure 5j), as foraminifera calcify at different depths during ontogeny it stands to reason that this can be used as a stratification index without the potential variability associated with ecological differences between different species. During the Glacial Ice rafting event HE 15, a larger temperature difference (2–3 °C) is observed with the $\Delta\delta^{18}O$ for both stratification indices (between *G. bulloides* and *G. inflate*, and small and large *G. inflata*). Following the termination, in which the maximum temperature difference occurs (~4 °C), this difference proceeds to decrease reaching a minimum at HE 14. This gradual decrease is also observed within the difference between small and large specimens of *G. inflata* (Figure 5j). The wind regime over this region of the North Atlantic is sensitive to the reduction in seasonal temperature extremes (Metcalfe et al., 2015); comparison with the pollen data in terrestrial records shows that periods of increased mixing during the interglacial coincide with forests extending into south-western Europe (e.g., Roucoux et al., 2006). Whereas, periods of enhanced stratification coincide with barren more arid conditions. Millennial-scale climate fluctuations, during MIS 7, have been likened to similar events during Termination I, that is, the Younger Dryas, using high-resolution pollen records from the Mediterranean (e.g., Fletcher et al., 2013).

4.2. *N. pachyderma* $\delta^{18}O$

Single-shell $\delta^{18}O$ analysis of *G. bulloides*, *G. inflata* (Metcalfe et al., 2015), and the coiling ratio (sinistral and dextral) of *G. truncatulinoides* (Feldmeijer et al., 2015) have been analyzed previously; here new single-shell $\delta^{18}O$ data of *N. pachyderma* were generated. *N. pachyderma* is an important indicator of "polar" conditions (Schiebel et al., 2017), being associated with the southward migration of the polar front during glacial conditions (Penaud et al., 2008; Ruddiman and McIntyre, 1981) and its occurrence either precedes or follows ice-rafting during Heinrich events (Kretschmer et al., 2016). As it is considered one of the "coldest" it is therefore often used as an end-member for understanding such extreme conditions (Cortijo et al., 1997; Roche et al., 2004), making it a logical target for $\sigma\delta^{18}O$ during glacial conditions. Of the three extant neogloboquanids, the left-coiling *N. pachyderma* differs from the right-coiling form *N. incompta* (Figure 2) and the subtropical symbiotic *Neogloboquadrina dutertrei* (Bird et al., 2018) with respect to temperature, salinity, and aspects of its calcification. For instance, *N. pachyderma*'s ability to be incorporated into sea ice, potentially surviving in brine channels, combined with occurrence in seasonal meltwater suggests a tolerance for extremes in salinity (Lipps & Krebbs, 1974; Spindler & Dieckmann, 1986). The species is capable of calcifying between −2 °C and either 10 or 12 °C (depending on whether winter, summer, or annual SST is used as a comparison; Eynaud, 2011) dominating polar sediments (Imbrie & Kipp, 1971; Kipp, 1976; Pflaumann et al., 1996). The extreme limits of the species distribution have been suggested as far as 25°S and 25°N (Kennett & Srinivasan, 1980), although it has made occurrences at lower latitudes (Parker, 1962; Zobel, 1973), most notably in upwelling regions (Ivanova et al., 1999; Ufkes et al., 1998; Ufkes & Zachariasse, 1993). While there is an indication that morphological variation occurs with environmental conditions (Altuna et al., 2018) and temperature (Kennett, 1968; Moller et al., 2013), a critical change is the coiling ratio from the predominately sinistral coiling *N. pachyderma* to the predominately dextral coiling *N. incompta* with increasing temperature (Bandy, 1959, 1960; Ericson, 1959). The change in proportion of sinistral and dextral coiling forms, now recognized as two discrete species (Cifelli, 1961, 1965; Cifelli & Smith, 1970; Darling et al., 2006), provides an additional paleoceanographic tool (Bandy, 1959, 1960; Darling et al., 2006; Ericson, 1959). In our record, this ratio shifts from ~2 to ~87% corresponding in the modern ocean to a mean annual temperature range between 5< and >10 °C, and thus, when conditions vary between the polar and subtropical water

masses this proportion can be used to estimate the mean annual average SST (Darling et al., 2006). In combination with the coiling ratio, isotopic shifts can be inferred to be either actual temperature shifts or meltwater events and therefore seasonal changes tracked through both intraspecies variability and interspecies offsets.

Here the standard deviation of *N. pachyderma* and the isotopic difference between *N. incompta* and *N. pachyderma* are used as a measure of the extent of both the growing season and the seasonal contrast (Figure 6). Pooled $\delta^{18}O$ analysis of *N. incompta* and single $\delta^{18}O$ *N. pachyderma* allows for the computation of the difference ($\Delta\delta^{18}O$) between the means. The upper temperature limit of *N. pachyderma* has been suggested to be ~10 °C (Lombard et al., 2009; Lombard et al., 2011; Roche et al., 2018), with the coiling ratio being dominated by *N. pachyderma* below 5 °C (Darling et al., 2006). If the major difference in species ecology is temperature, then the $\Delta\delta^{18}O$ between coexisting specimens of *N. incompta* and *N. pachyderma* $\delta^{18}O$ (Figure 5d) should represent a temperature signal, and the $\sigma\delta^{18}O$ (Figure 5c) the magnitude of the seasonality (Figure 6). This is likely a relative proxy, limited to the overlap that exists between the temperature tolerances of both species, that is, between ~5 and ~10 °C (Lombard et al., 2009; Lombard et al., 2011; Roche et al., 2018). Across the whole record these parameters ($\Delta\delta^{18}O$ versus $\sigma\delta^{18}O_{NPS}$) show a negative linear relationship with large isotopic differences associated with small standard deviations in *N. pachyderma* and vice versa, which has an r^2 of 0.45 ($n = 26$; yellow line Figure 6d). The two samples with the largest $\sigma\delta^{18}O$ (>0.8‰) also reflect the two samples with the lowest percentage of *N. pachyderma* (Figure 5a); anectodical evidence suggests that when the abundance of *N. pachyderma* is low it may represent a different form of *N. incompta* (and vice versa), although no proof (e.g., genetic studies) beyond anecdotes exist for such claims. Removal of these two points would increase the r^2 to 0.51 ($n = 24$; blue line in Figure 6d). Plotting a modern core top sample, here Actuomicropaleontology Paleoceanography North Atlantic Project I (Ganssen et al., 1991; Ganssen & Kroon, 2000; Troelstra et al., 1987) T86-5B (46°53′N, 25°21′W; water depth 3,121 m), using either the standard deviation of *N. incompta* and *N. pachyderma* with $n = 20$ and 5, respectively (red circles representing the same data plotted with different circumstance; Figure 6), shows that samples with low percentage of *N. pachyderma* plot with a large standard deviation. If the extreme data points ($\sigma\delta^{18}O > 0.8$‰) are ignored, then there appears to be little change with $\Delta\delta^{18}O$ values <0.50‰ (Figure 6d).

While our interpretation is based upon the $\Delta\delta^{18}O$ reflecting a temperature difference between *N. pachyderma* and *N. incompta*, given the fact that the coiling ratio between the two is generally used as a temperature proxy, of course, temperature is only one aspect responsible for changes and variation in $\Delta\delta^{18}O$ and $\delta^{18}O$. Detecting absolute temperature changes from the $\delta^{18}O$ in foraminiferal shells alone is not possible. While the ambient temperature during calcification influences $\delta^{18}O_c$, it is also affected by the ambient seawater signal ($\delta^{18}O_{sw}$), which is itself a product of both water mass history (e.g., evaporation, precipitation, dilution) and global ice volume ($\delta^{18}O_{IVE}$). Furthermore, potential disequilibrium processes during calcification, commonly referred to as the vital effect and postmortem effects (i.e., dissolution or bioturbation), serve to further alter the signal premortem or postmortem. In section 4.3, we elaborate upon the potential influence of bioturbation, although it is worth noting here that previous work (Feldmeijer et al., 2015) does suggest that the influence of bioturbation upon this section of T90-9P is not as extreme as in other cases (Lougheed et al., 2018; Wit et al., 2013), although appearances can be deceiving. This leaves either vital effect or the influence of salinity. There is a discrepancy in the literature regarding whether *N. pachyderma* calcifies in equilibrium ($\delta^{18}O_{eq}$); such equilibrium calcification would be indicative of either a minor or no vital effect. Estimates of the oxygen isotopic offset for *N. pachyderma* range from 0.8‰ to no offset to −0.45‰ (Duplessy et al., 1988; Kellogg et al., 1978; Kohfeld et al., 1996; Spielhagen & Erlenkeuser, 1994); such a considerably large range could reflect discrepancies in accounting for secondary calcification (Kennett & Srinivasan, 1980; Srinivasan & Kennett, 1974), which may shift the signal deeper in the water column reducing the influence of surface perturbations (Kohfeld et al., 1996; Roche et al., 2018). However, if vital effect remains constant, for example, that biological and calcification processes do not vary along a species environmental gradient, then vital effect as an argument can be discounted. If the two species are known to be separated ecologically and the vital effect is constant, then the difference can be written as $\Delta\delta^{18}O = \delta^{18}O_{Species\ a} - \delta^{18}O_{Species\ b}$, where both $\delta^{18}O_{Species\ a}$ and $\delta^{18}O_{Species\ b}$ are equal to $\delta^{18}O_{Species\ i} = \delta^{18}O_{eq} + \delta^{18}O_{VE\ (Species\ i)}$; effectively, the $\delta^{18}O_{VE}$ terms "cancel" one another out. The vital effect may serve to mute or exaggerate the actual difference between two species, but if it

remains constant then it cannot explain the change in $\Delta\delta^{18}O$ through time. This leaves salinity; evidence suggests that despite the $\delta^{18}O$ being unaffected by melting sea ice, core top samples of *N. pachyderma* measured by Spielhagen and Erlenkeuser (1994) have shown a relationship with salinity. Does this invalidate the potential for interpreting a seasonal, or interannual, separation between *N. pachyderma* and *N. incompta*? It seems unlikely. The species *N. pachyderma* is an indicator of subpolar to polar colder and fresher water masses, whereas *N. incompta* is a species that inhabits warmer environments (Cifelli, 1961, 1965; Cifelli & Smith, 1970). Therefore, it could equally be possible that changes and variation in $\delta^{18}O$, $\Delta\delta^{18}O$, and $\sigma\delta^{18}O$ are capturing distinct water masses (e.g., freshwater-meltwater). The $\sigma\delta^{18}O$ could then reflect different distinct periods, that is, sea ice formation and melting, and the $\Delta\delta^{18}O$ the difference between open ocean conditions and conditions with ice. The absolute value and sign of the deviation between the two species would then depend not only on the initial $\delta^{18}O_{sw}$ but whether the population calcifies in the seawater where sea ice is forming, or where sea ice or icebergs are melting. It is interesting that the ratio between *N. pachyderma* and *N. incompta*, a temperature indicator (Darling et al., 2006), and the oxygen isotope composition of the species are not in sync (Kohfeld et al., 1996). This could reflect changes in $\delta^{18}O_{sw}$ that alter the $\delta^{18}O$ of *N. pachyderma*. Theoretically, the $\delta^{18}O_{sw}$ could be calculated by rearranging the paleotemperature equation to solve for $\delta^{18}O_{sw}$ (e.g., de Vernal and Hillaire-Marcel 2006 or Hillaire-Marcel et al. 2004). One problem, however, with using the coiling ratio to causally infer temperature shifts or meltwater events is that it is an estimate of annual average SST (Darling et al., 2006) and the actual seasonally weighted $\delta^{18}O_c$ may be considerably different (Jonkers & Kucera, 2017; Mix, 1987; Roche et al., 2018), further complicated by seasonal meltwater-induced changes in $\delta^{18}O_{sw}$.

Taking these points into consideration, the neogloboquadrinid data, wherein the $\Delta\delta^{18}O$ and $\sigma\delta^{18}O$ correlate, can be interpreted in the following way. It is plausible that during the meltwater event at 250 and 242 kyr, conditions favored the cold *N. pachyderma* increasing its growing season and marginalizing the warmer *N. incompta* which likely obscured the meltwater spike. Following this event these proxies show that temperature declines even after the apparent ice volume maxima at 242 kyr, based upon $\delta^{18}O$ of *C. wuellerstorfi* (Figure 5m), until the termination at 230 kyr. Between 230 and 218 kyr the $\delta^{18}O$ of *N. pachyderma* and coiling ratio diverge, likely indicating an increase in ice volume between 230 and 226 kyr during the rise in temperatures followed by a decrease at 226 kyr. The onset of the HE (~210 kyr) during the cold stage of MIS 7d occurs with a drop-in temperature prior to a meltwater spike, although this is smaller in amplitude than the preceding, HE during MIS 8, taking the coiling ratio (Figure 5b) as a measure. Between 250 and 242 kyr the depletion in oxygen isotopes, following the peak in IRD (Figure 5e), appears synchronous with a shift in the coiling ratio (Figure 5b). This implies that the HE likely led to cooling as well as a freshening of the North Atlantic.

It is important to note that the $\sigma\delta^{18}O$ of *N. pachyderma* does not correlate with either the insolation, or the summer-winter insolation difference; this could be the result of the upper temperature limit of this species restricting the response detectable at our core site. A return to conditions similar to the present day, during the interglacial of MIS 7, would shift the biogeography of *N. pachyderma* poleward and away from the core location (Wolfteich, 1994) which could explain why despite a correlation with *N. incompta* there is no correlation with insolation (Figure 5). As conditions improved, and temperatures warmed, *N. pachyderma* would have been outcompeted by *N. incompta* and other warmer species (*N. pachyderma* > *N. incompta* > *G. bulloides* > *G. ruber*). Likewise, as conditions deteriorated, it is likely that ecological space of *N. pachyderma* was limited by a reduction in food. While this would appear to hamper the usefulness of this as a proxy, it is worth considering this with respect to the location of the core site, analysis of cores at higher latitudes where *N. pachyderma*'s presence is continuous between glacial and interglacial conditions could be used to further test this proxy. Regardless, in order to compensate for this the $\sigma\delta^{18}O$ of *G. bulloides* (Metcalfe et al., 2015; Figures 3 and 4) was utilized to test the relationship between insolation and foraminiferal $\sigma\delta^{18}O$. It is worth noting that the increase in *G. bulloides* $\sigma\delta^{18}O$ coincides with an increase in the abundance of *G. ruber*, and as *G. ruber* is a subtropical to tropical species, it suggests either warmer conditions or the advection of a warm water mass, the occurrence of warmer conditions that maybe more favorable to *G. bulloides* than *N. pachyderma* (Figure 5k), supporting our inference regarding the mismatch between *N. pachyderma* $\sigma\delta^{18}O$ and insolation. The shift in both the abundance (Figure 5l) and the oxygen isotopic standard deviation ($\sigma\delta^{18}O$) of *G. bulloides* does correspond to a change in the insolation difference

between July and December (Figure 5g; Metcalfe et al., 2015). In order to explain why an increase in insolation may have a negative correlation let us consider that the annual surface temperature profile of a core site can be approximated by a sine wave (Figure 6a), as such the temperature can be high (red curve) or low amplitude (black) and these have specific distributions (Figures 6b and 6c). Intriguingly such a distribution is not a normal distribution, as per Mix (1987), instead having two high-frequency peaks at either end (Figure 6c; Metcalfe et al., 2015). These specific distributions highlight one aspect of seasonality; a high-amplitude distribution (red) will have a larger overall range in temperature, but a reduced frequency at each point in temperature compared to a lower amplitude distribution (black). When the insolation difference between July and December is small, the $\sigma\delta^{18}O$ of *G. bulloides* is larger; if we take our low amplitude as an example, there is higher frequency (i.e., greater "number of days") at each particular temperature. While this appears counterintuitive, in the modern North Atlantic Ocean *G. bulloides* is dependent upon conditions that trigger the spring bloom (Ganssen & Kroon, 2000). Winter mixing of the water column allows for the replenishment of nutrients exhausted during summer stratification, creating the foundation of a formation of a phytoplankton bloom that acts as a food source for *G. bulloides*. During periods of enhanced seasonality, it is hypothesized that the stratification that exists during the summer months was stronger, leading to longer nutrient-depleted periods. This means that when the two (summer and winter) insolation parameters are at maximum values in the midlatitude North Atlantic, that is, the difference between the two seasons is greatest, the growing season is reduced (higher amplitude sine curve; Figure 6).

4.3. Implications: Proxy and Sedimentological Artifacts

Irrespective of our interpretations our results highlight three important aspects: (1) the first is the complexity involved with the multispecies $\delta^{18}O$ approach (Figure 4). The complexity of multispecies $\delta^{18}O$ can be seen if one considers the data at T-III, an abrupt transition; our multispecies $\delta^{18}O$ highlights discrepancies that cannot be explained purely by depth preferences. For instance, *G. truncatulinoides* (Figure 4a), the planktonic foraminifera with the deepest depth preference, has a similar abrupt signal as the cosmopolitan *G. glutinata*, whereas both *G. inflata* and *N. incompta* have an apparently more "muted" signal across the transition (Figure 4b). While bioturbation is not species-specific, it may have different impacts upon different species (Bard, Arnold, Duprat, et al., 1987a, 1987b; Bard, Arnold, Maurice, et al., 1987), especially when considering the finite sampling of paleoceanography. Depending on the intensity of bioturbation, the mixing of species that are abundant versus species that are scarce may give rise to the apparent appearance of bioturbation overtly influencing one species more than another, weakening or strengthening the contrast between samples, especially if the analysis uses too few specimens. However, in reality, the sediment is equally bioturbated. Previous work (Feldmeijer et al., 2015) gives us confidence that bioturbation has not unduly influenced this section of T90-9P. Therefore, it must be considered that a reason for a lack of coherence between species is that superimposed upon the climate signal is species-specific variability (Mix, 1987; Mulitza et al., 1998; Roche et al., 2018), a function of the unique behavior of a species and the interplay between predators and prey and/or interspecific and intraspecific competition. It does raise the question whether there are any stratigraphic features that represent species traits rather than attributable climatic events, and what makes for a better species for stratigraphic purposes: a species with a sensitivity to regional events, that is, *N. pachyderma*, or one that records climate extremes, that is, the cosmopolitan *G. glutinata* or deep-dweller *G. truncatulinoides*.

The (2) second important aspect is the potential problem in viewing the various species in isolation or as isolated facets of the climate system (Figure 6). Here the relationship between *N. pachyderma* and *N. incompta* is further examined, resulting in the detection of a correlation between $\Delta\delta^{18}O$ and $\sigma\delta^{18}O$. Species with similar ecological niches are likely to have some interplay over climate transitions, as subtle changes in conditions (e.g., temperature or food source) may favor certain species over others. Such relationships between species can be advantageous; for instance, in previous work the fact that monsoonal conditions favor one species on another has allowed for the full seasonal range to be computed (Ganssen et al., 2011). Establishing more detailed ecological information (e.g., food, feeding rate, population carrying capacity) beyond the current environmental information (i.e., temperature, salinity) would allow for more accurate climate reconstructions.

Finally, the (3) third important aspect is the "hidden variance" downcore, emphasized by both the raw shell measurements (Figure 3) and the variability between samples of species specific $\sigma\delta^{18}O$ (Figures 5 and 6).

While the data presented here could be considered as low resolution spatially (one sample every 4 cm; Table 1) or temporally (one sample every ~1 to 2 kyr; Figures 3–5 and Table 1), we have opted for a higher density of sample points (n = 6,266) concentrated in a fewer cm (n = 26). The range in $\delta^{18}O$ of a single species (Figures 3 and 4) is an order of magnitude larger than the accuracy and precision associated through replicate analysis of in-house and/or international standards. It is worth noting that the spread in foraminiferal values is generally considered to be an underrepresentation of the total seasonal signal, either because foraminifera have a monthly life cycle (Hemleben et al., 1989; Spindler et al., 1979); the flux of all or a particular species of foraminifera is limited to a particular season (Mix, 1987; Roche et al., 2018); or the sedimentology of the core is unrepresentative (i.e., a slow sedimentation accumulation rate). One benefit of such analysis is that the individual specimen's $\delta^{18}O$ can be considered by the researcher prior to the calculation of a mean $\delta^{18}O$; anomalous values can be screened via outlier analysis (Ganssen et al., 2011) or through "unmixing" of the sample into discrete subsamples representing specimens from unique populations (Wit et al., 2013) so that a more robust downcore species-specific $\delta^{18}O$ can be produced. In combination with other analytical techniques, such as photographing and weighing of shells (e.g., Altuna et al., 2018; Pracht et al., 2018) prior to analysis or removing a portion of the shell for radiocarbon analysis, taxonomic issues (Pracht et al., 2018) and benthic processes (Lougheed et al., 2018) can be nullified or subsequently corrected. While the range in minimum and maximum values of single-shell $\delta^{18}O$ (Figures 4c–4e) is a useful first approach, it is unlikely indicative of solely bioturbation, being a function of the time period encapsulated within the sample, the degree of interannual variability (e.g., El Niño–Southern Oscillation) and whether the sample is in a climatological plateau (e.g., the Holocene, wherein bioturbation in a "stable" climate is undetectable by $\delta^{18}O$ because of similar $\delta^{18}O$ values). What is evident, however, in the range of single-shell $\delta^{18}O$ (Figures 4c–4e) is the amount of information lost through continued use of pooled specimen analysis and the potential for replication error should the number of specimens within a "pool" be inadequate (Morard et al., 2016). While attempts at obtaining a more robust average include crushing a larger subset of specimens than necessary and analyzing a series of crushed sample replicates (e.g., Scussolini & Peeters, 2013) inclusion of bioturbated or anomalous specimens into a pooled analysis cannot be subsequently remedied. Systematic bioturbation caused by the constant presence of a sedimentary mixed layer throughout the history of the sediment retrieved via coring will smooth out the true variation of the pooled specimen signal. Single-specimen analysis therefore sheds light on the true variation of the paleoceanographic signal; further work is required to better understand the processes involved (Dolman & Laepple, 2018; Roche et al., 2018) to enable more accurate interpretations.

5. Conclusions

Seasonality is an important parameter when deducing the climate of the past. The spread in oxygen isotope values from single-shell analysis ($\sigma(\delta^{18}O)$) have been used as an indicator of a populations seasonal and/or depth habitat. Here the $\delta^{18}O$ values of *N. pachyderma* from MIS 8 and MIS 7 were analyzed and in combination with pooled benthic (*C. wuellerstorfi*) and planktonic (*G. glutinata* and *N. incompta*) foraminifera $\delta^{18}O$ compared with existing *G. bulloides*, *G. inflata*, and *G. truncatulinoides* $\delta^{18}O$ data. Our results highlight the interrupted nature of T-III and the sporadic return to near glacial conditions during MIS 7, identifying three (two Heinrich style events and one Termination Ice Rafting Event) ice rafting events that occur during and between MIS 8 and 7. With respect to seasonality we highlight the fact that the oxygen isotopic difference between *N. pachyderma* and *N. incompta* ($\Delta\delta^{18}O$) correlates with the $\sigma\delta^{18}O$ of *N. pachyderma*, a measure of the spread. This can be explained as a measure of the size of ecological space (either the result of seasonality in temperature or salinity) and the degree of overlap and variability of the growing season of the cold species *N. pachyderma* and *N. incompta*. However, the $\sigma\delta^{18}O$ of *N. pachyderma* does not appear to relate to insolation at the core site, while we cannot explicitly rule out benthic processes such as bioturbation; this is potentially the result of the conditions at the core site exceeding the upper temperature limit of *N. pachyderma*. In an attempt to bypass this problem, the $\sigma\delta^{18}O$ of *G. bulloides*, a species that is continuously present throughout MIS 8 and MIS 7, was utilized. Our results suggest that the $\sigma\delta^{18}O$ of *G. bulloides* relates to insolation and thus can be used as a proxy for seasonality. As the difference in summer and winter insolation increased, curiously the $\sigma\delta^{18}O$ of *G. bulloides* decreased likely a reflection of a reduced habitat.

Acknowledgments

This work is part of the research program "Digging for Density" with project NWO/822.01.0.19, which is financed by the Netherlands Organization for Scientific Research (NWO). The authors acknowledge the Darwin Center for Biogeosciences Theme 2 project "Sensing Seasonality" with project 3043, which partially funded this project, and the European 7th Framework Project European Project for Ocean Acidification (EPOCA; FP7/211384). B.M. is supported by a Laboratoire d'Excellence (LabEx) award from the Institut Pierre-Simon Laplace (IPSL). Data are available in Table 1.

References

Altuna, N. E. B., Pieńkowski, A. J., Eynaud, F., & Thiessen, R. (2018). The morphotypes of Neogloboquadrina pachyderma: Isotopic signature and distribution patterns in the Canadian Arctic Archipelago and adjacent regions. *Marine Micropaleontology*, *142*, 13–24. https://doi.org/10.1016/j.marmicro.2018.05.004

Bandy, O. L. (1959). The geologic significance of coiling ratios in the foraminifer *Globigerina pachyderma* (Ehrenberg). *Geological Society of America Bulletin*, *70*, 1708.

Bandy, O. L. (1960). The geologic significance of coiling ratios in the foraminifer *Globigerina pachyderma* (Ehrenberg). *Journal of Paleontology*, *34*, 671–681.

Bard, E., Arnold, M., Duprat, J., Moyes, J., & Duplessy, J. C. (1987a). Bioturbation effects on abrupt climatic changes recorded in deep sea sediments. Correlation between $\delta^{18}O$ profiles and accelerator ^{14}C dating. In W. H. Berger & L. D. Labeyrie (Eds.), *Abrupt Climatic Change: Evidence and Implications* (pp. 263–278). Dordrecht, Netherlands: Springer. https://doi.org/10.1007/978-94-009-3993-6_24

Bard, E., Arnold, M., Duprat, J., Moyes, J., & Duplessy, J.-C. (1987b). Reconstruction of the last deglaciation: Deconvolved records of $\delta^{18}O$ profiles, micropaleontological variations and accelerator mass spectrometric ^{14}C dating. *Climate Dynamics*, *1*(2), 101–112. https://doi.org/10.1007/BF01054479

Bard, E., Arnold, M., Maurice, P., Duprat, J., Moyes, J., & Duplessy, J.-C. (1987). Retreat velocity of the North Atlantic polar front during the last deglaciation determined by ^{14}C accelerator mass spectrometry. *Nature*, *328*(6133), 791–794. https://doi.org/10.1038/328791a0

Bird, C., Darling, K. F., Russell, A. D., Fehrenbacher, J. S., Davis, C. V., Free, A., & Ngwenya, B. T. (2018). 16S rRNA gene metabarcoding and TEM reveals different ecological strategies within the genus *Neogloboquadrina* (planktonic foraminifer). *PLoS ONE*, *13*(1), e0191653. https://doi.org/10.1371/journal.pone.0191653

Cheng, H., Edwards, R. L., Broecker, W. S., Denton, G. H., Kong, X., Wang, Y., et al. (2009). Ice age terminations. *Science*, *326*(5950), 248–252. https://doi.org/10.1126/science.1177840

Chiang, J. C. H., & Bitz, C. M. (2005). Influence of high latitude ice cover on the marine Intertropical Convergence Zone. *Climate Dynamics*, *25*(5), 477–496. https://doi.org/10.1007/s00382-005-0040-5

Cifelli, R. (1961). *Globigerina incompta*, a new species of pelagic foraminifera from the North Atlantic. *Contributions from the Cushman Foundation for Foraminiferal Research*, *7*(3), 83–86.

Cifelli, R. (1965). *Planktonic Foraminifera From the Western North Atlantic* (Vol. 148). Washington, DC: Smithsonian Institution.

Cifelli, R., & Smith, R. K. (1970). Distribution of planktonic foraminifera in the vicinity of the North Atlantic current. *Smithsonian Contributions to Paleobiology*, *4*, 51.

Cortijo, E., Labeyrie, L., Vidal, L., Vautravers, M., Chapman, M., Duplessy, J.-C., et al. (1997). Changes in sea surface hydrology associated with Heinrich event 4 in the North Atlantic Ocean between 40° and 60°N. *Earth and Planetary Science Letters*, *146*(1-2), 29–45. https://doi.org/10.1016/S0012-821X(96)00217-8

Darling, K. F., Kucera, M., Kroon, D., & Wade, C. M. (2006). A resolution for the coiling direction paradox in *Neogloboquadrina pachyderma*. *Paleoceanography*, *21*, PA2011. https://doi.org/10.1029/2005PA001189

de Vernal, A., & Hillaire-Marcel, C. (2006). Provincialism in trends and high frequency changes in the Northwest North Atlantic during the Holocene. *Global and Planetary Change*, *54*(3-4), 263–290. https://doi.org/10.1016/j.gloplacha.2006.06.023

Denton, G. H., Alley, R. B., Comer, G. C., & Broecker, W. S. (2005). The role of seasonality in abrupt climate change. *Quaternary Science Reviews*, *24*(10–11), 1159–1182. https://doi.org/10.1016/j.quascirev.2004.12.002

Denton, G. H., Anderson, R. F., Toggweiler, J. R., Edwards, R. L., Schaefer, J. M., & Putnam, A. E. (2010). The last glacial termination. *Science*, *328*(5986), 1652–1656.

Dolman, A. M., & Laepple, T. (2018). Sedproxy: A forward model for sediment-archived climate proxies. *Climate of the Past*, *14*(12), 1851–1868. https://doi.org/10.5194/cp-14-1851-2018

Duplessy, J.-C., Labeyrie, L., & Blanc, P.-L. (1988). Norwegian Sea deep water variations over the last climatic cycle: Paleoceanographical implications. In H. Wanner, & U. Siegenthaler (Eds.), *Long and Short Term Variability of Climate* (pp. 83–116). Berlin: Springer. https://doi.org/10.1007/BFb0046591

Emiliani, C. (1954). Depth habitats of some species of pelagic foraminifera as indicated by oxygen isotope ratios. *American Journal of Science*, *252*(3), 149–158. https://doi.org/10.2475/ajs.252.3.149

Ericson, D. B. (1959). Coiling direction of *Globigerina pachyderma* as a climatic index. *Science*, *130*(3369), 219–220. https://doi.org/10.1126/science.130.3369.219

Eynaud, F. (2011). Planktonic foraminifera in the Arctic: potentials and issues regarding modern and quaternary populations. *IOP Conference Series: Earth and Environmental Science*, *14*, 012005. https://doi.org/10.1088/1755-1315/14/1/012005

Feldmeijer, W., Metcalfe, B., Brummer, G. J. A., & Ganssen, G. M. (2015). Reconstructing the depth of the permanent thermocline through the morphology and geochemistry of the deep dwelling planktonic foraminifer *Globorotalia truncatulinoides*. *Paleoceanography*, *30*, 1–22. https://doi.org/10.1002/2014PA002687

Fletcher, W. J., Müller, U. C., Koutsodendris, A., Christanis, K., & Pross, J. (2013). A centennial-scale record of vegetation and climate variability from 312 to 240 ka (marine isotope stages 9c–a, 8 and 7e) from Tenaghi Philippon, NE Greece. *Quaternary Science Reviews*, *78*, 108–125. https://doi.org/10.1016/j.quascirev.2013.08.005

Ganssen, G. M., & Kroon, D. (2000). The isotopic signature of planktonic foraminifera from NE Atlantic surface sediments: Implications for the reconstruction of past oceanic conditions. *Journal of the Geological Society*, *157*(3), 693–699. https://doi.org/10.1144/jgs.157.3.693

Ganssen, G. M., Peeters, F., Metcalfe, B., Anand, P., Jung, S., Kroon, D., & Brummer, G. (2011). Quantifying Sea surface temperature ranges of the Arabian Sea for the past 20,000 years. *Climate of the Past*, *7*(4), 1337–1349. https://doi.org/10.5194/cp-7-1337-2011

Ganssen, G. M., Troelstra, S., van der Borg, K., & De Jong, A. M. F. (1991). Late Quarternary Pteropod preservation in eastern North Atlantic sediments in relation to changing climate. *Radiocarbon*, *33*(03), 277–282. https://doi.org/10.1017/S0033822200040297

Gruber, N., Keeling, C. D., & Bates, N. R. (2002). Interannual variability in the North Atlantic Ocean carbon sink. *Science*, *298*(5602), 2374–2378. https://doi.org/10.1126/science.1077077

Hemleben, C., Spindler, M., & Anderson, O. R. (1989). *Modern Planktonic Foraminifera*. New York: Springer-Verlag. https://doi.org/10.1007/978-1-4612-3544-6

Hillaire-Marcel, C., de Vernal, A., Polyak, L., & Darby, D. (2004). Size-dependent isotopic composition of planktic foraminifers from Chukchi Sea vs. NW Atlantic sediments—Implications for the Holocene paleoceanography of the western Arctic. *Quaternary Science Reviews*, *23*(3-4), 245–260. https://doi.org/10.1016/j.quascirev.2003.08.006

Huybers, P. (2007). Glacial variability over the last two million years: An extended depth-derived age model, continuous obliquity pacing, and the Pleistocene progression. *Quaternary Science Reviews*, *26*(1–2), 37–55. https://doi.org/10.1016/j.quascirev.2006.07.013

Huybers, P., & Wunsch, C. (2004). A depth-derived Pleistocene age model: Uncertainty estimates, sedimentation variability, and nonlinear climate change. *Paleoceanography*, *19*, PA1028. https://doi.org/10.1029/2002PA000857

Imbrie, J., & Kipp, N. G. (1971). A new micropaleontological method for paleoclimatology: Application to a Late Pleistocene Caribbean core. In K. K. Turekian (Ed.), *The Late Cenozoic Glacial Ages* (pp. 71–181). New Haven, Connecticut: Yale University Press.

Isarin, R. F. B., & Renssen, H. (1999). Reconstructing and modelling late Weichselian climates: The Younger Dryas in Europe as a case study. *Earth-Science Reviews*, *48*(1–2), 1–38. https://doi.org/10.1016/S0012-8252(99)00047-1

Isarin, R. F. B., Renssen, H., & Vandenberghe, J. (1998). The impact of the North Atlantic Ocean on the Younger Dryas climate in north-western and central Europe. *Journal of Quaternary Science*, *13*(5), 447–453. https://doi.org/10.1002/(SICI)1099-1417(1998090)13:5<447::AID-JQS402>3.0.CO;2-B

Isarin, R. F. B., Renssen, H., & Vandenberghe, J. (1999). The impact of the North Atlantic Ocean on the Younger Dryas climate in north-western and central Europe. *Journal of Quaternary Science*, *13*(5), 447–453. https://doi.org/10.1002/(SICI)1099-1417(1998090)13:5<447::AID-JQS402>3.0.CO;2-B

Ishimura, T., Tsunogai, U., & Nakagawa, F. (2008). Grain-scale heterogeneities in the stable carbon and oxygen isotopic compositions of the international standard calcite materials (NBS 19, NBS 18, IAEA-CO-1, and IAEA-CO-8). *Rapid Communications in Mass Spectrometry*, *22*(12), 1925–1932. https://doi.org/10.1002/rcm.3571

Ivanova, E. M., Conan, S. M.-H., Peeters, F. J. C., & Troelstra, S. R. (1999). Living *Neogloboquadrina pachyderma* sin and its distribution in the sediments from Oman and Somalia upwelling areas. *Marine Micropaleontology*, *36*(2–3), 91–107. https://doi.org/10.1016/S0377-8398(98)00027-9

Jonkers, L., & Kucera, M. (2017). Quantifying the effect of seasonal and vertical habitat tracking on planktonic foraminifera proxies. *Climate of the Past*, *13*(6), 573–586. https://doi.org/10.5194/cp-13-573-2017

Kellogg, T. B., Duplessy, J.-C., & Shackleton, N. J. (1978). Planktonic foraminiferal and oxygen isotopic stratigraphy and paleoclimatology of Norwegian Sea deep-sea cores. *Boreas*, *7*(1), 61–73. https://doi.org/10.1111/j.1502-3885.1978.tb00051.x

Kennett, J. P. (1968). Latitudinal variation in *Globigerina pachyderma* (Ehrenberg) in surface sediments of the Southwest Pacific Ocean. *Micropaleontology*, *14*(3), 305–318. https://doi.org/10.2307/1484691

Kennett, J. P., & Srinivasan, M. S. (1980). Surface ultrastructural variation in *Neogloboquadrina pachyderma* (Ehrenberg): Phenotypic variation and phylogeny in the late Cenozoic. In W. V. Sliter, J. C. Ingle, J. P. Kennett, R. Kolpack, & E. Vincent (Eds.), *Studies in Marine Micropaleontology and Paleoecology: A Memorial Volume to Orville l. Bandy* (pp. 134–162). Lawrence, Kansas (USA): Cushman Foundation for Foraminiferal Research, Allen Press.

Kim, S.-T., & O'Neil, J. R. (1997). Equilibrium and nonequilibrium oxygen isotope effects in synthetic carbonates. *Geochimica et Cosmochimica Acta*, *61*(16), 3461–3475. https://doi.org/10.1016/S0016-7037(97)00169-5

Kipp, N. G. (1976). New transfer function for estimating past sea-surface conditions from sea-bed distribution of planktonic foraminiferal assemblages in the North Atlantic. In R. M. Cune & J. D. Hays (Eds.), *Investigation of Late Quaternary Paleoceanography and Paleoclimatology* (Vol. 145, pp. 3–42). Retrieved from https://doi.org/10.1130/MEM145-p3

Kohfeld, K. E., Fairbanks, R. G., Smith, S. L., & Walsh, I. D. (1996). *Neogloboquadrina pachyderma* (sinistral coiling) as paleoceanographic tracers in polar oceans: Evidence from northeast water polynya plankton tows, sediment traps, and surface sediments. *Paleoceanography*, *11*(6), 679–699. https://doi.org/10.1029/96PA02617

Koutavas, A., deMenocal, P. B., Olive Col, G. C., & Lynch-Stieglitz, J. (2006). Mid-Holocene El Niño–Southern Oscillation (ENSO) attenuation revealed by individual foraminifera in eastern tropical Pacific sediments. *Geology*, *34*(12), 993–996. https://doi.org/10.1130/G22810A.1

Koutavas, A., & Joanides, S. (2012). El Niño–Southern Oscillation extrema in the Holocene and last glacial maximum. *Paleoceanography*, *27*, PA4208. https://doi.org/10.1029/2012PA002378

Kretschmer, K., Kucera, M., & Schulz, M. (2016). Modeling the distribution and seasonality of *Neogloboquadrina pachyderma* in the North Atlantic Ocean during Heinrich Stadial 1. *Paleoceanography*, *31*, 986–1010. https://doi.org/10.1002/2015PA002819

Lang, N., & Wolff, E. W. (2011). Interglacial and glacial variability from the last 800 ka in marine, ice and terrestrial archives. *Climate of the Past*, *7*(2), 361–380. https://doi.org/10.5194/cp-7-361-2011

Leduc, G., Vidal, L., Cartapanis, O., & Bard, E. (2009). Modes of eastern equatorial Pacific thermocline variability: Implications for ENSO dynamics over the last glacial period. *Paleoceanography*, *24*, PA3202. https://doi.org/10.1029/2008PA001701

Lipps, J. H., & Krebbs, W. N. (1974). Planktonic foraminifera associated with Antarctic sea-ice. *Journal of Foraminiferal Research*, *4*(2), 80–85. https://doi.org/10.2113/gsjfr.4.2.80

Lombard, F., Labeyrie, L., Michel, E., Bopp, L., Cortijo, E., Retailleau, S., Howa, H., et al. (2011). Modelling planktic foraminifer growth and distribution using an ecophysiological multi-species approach. *Biogeosciences*, *8*(4), 853–873. https://doi.org/10.5194/bg-8-853-2011

Lombard, F., Labeyrie, L., Michel, E., Spero, H. J., & Lea, D. W. (2009). Modelling the temperature dependent growth rates of planktic foraminfera. *Marine Micropaleontology*, *70*(1-2), 1–7. https://doi.org/10.1016/j.marmicro.2008.09.004

Lototskaya, A., & Ganssen, G. M. (1999). The structure of termination II (penultimate deglaciation and Eemian) in the North Atlantic. *Quaternary Science Reviews*, *18*(14), 1641–1654. https://doi.org/10.1016/S0277-3791(99)00011-6

Lototskaya, A., Ziveri, P., Ganssen, G. M., & van Hinte, J. E. (1998). Calcareous nannofloral response to termination II at 45°N, 25°W (Northeast Atlantic). *Marine Micropaleontology*, *34*(1–2), 47–70. https://doi.org/10.1016/S0377-8398(98)00005-X

Lougheed, B. C., Metcalfe, B., Ninnemann, U. S., & Wacker, L. (2018). Moving beyond the age depth model paradigm in deep-sea palaeoclimate archives: Dual radiocarbon and stable isotope analysis on single foraminifera. *Climate of the Past*, *14*(4), 515–526. https://doi.org/10.5194/cp-14-515-2018

Metcalfe, B., Feldmeijer, W., de Vringer-Picon, M., Brummer, G. J. A., Peeters, F. J. C., & Ganssen, G. M. (2015). Late Pleistocene glacial–interglacial shell-size–isotope variability in planktonic foraminifera as a function of local hydrography. *Biogeosciences*, *12*(15), 4781–4807. https://doi.org/10.5194/bg-12-4781-2015

Mix, A. C. (1987). The oxygen-isotope record of deglaciation, in: North America and adjacent oceans during the last deglaciation. In W. F. Ruddiman & H. E. J. Wright (Eds.), *The Geology of America* (Vol. K-3, pp. 111–135). Boulder, CO: Geological Society of America.

Moller, T., Schulz, H., & Kucera, M. (2013). The effect of sea surface properties on shell morphology and size of the planktonic foraminifer *Neogloboquadrina pachyderma* in the North Atlantic. *Palaeogeography, Palaeoclimatology, Palaeoecology*, *391*, 34–48. https://doi.org/10.1016/j.palaeo.2011.08.014

Morard, R., Reinelt, M., Chiessi, C. M., Groeneveld, J., & Kucera, M. (2016). Tracing shifts of oceanic fronts using the cryptic diversity of the planktonic foraminifera *Globorotalia inflata*. *Paleoceanography*, *31*, 1193–1205. https://doi.org/10.1002/2016PA002977

Mulitza, S., Dürkoop, A., Hale, W., Wefer, G., & Stefan Niebler, H. (1997). Planktonic foraminifera as recorders of past surface-water stratification. *Geology*, *25*(4), 335–338. https://doi.org/10.1130/0091-7613(1997)025<0335:PFAROP>2.3.CO;2

Mulitza, S., Wolff, T., Pätzold, J., Hale, W., & Wefer, G. (1998). Temperature sensitivity of planktic foraminifera and its influence on the oxygen isotope record. *Marine Micropaleontology*, *33*(3–4), 223–240. https://doi.org/10.1016/S0377-8398(97)00040-6

Obrochta, S. P., Crowley, T. J., Channell, J. E. T., Hodell, D. A., Baker, P. A., Seki, A., & Yokoyama, Y. (2014). Climate variability and ice-sheet dynamics during the last three glaciations. *Earth and Planetary Science Letters*, *406*, 198–212. https://doi.org/10.1016/j.epsl.2014.09.004

Olson, P., Reynolds, E., Hinnov, L., & Goswami, A. (2016). Variation of ocean sediment thickness with crustal age. *Geochemistry, Geophysics, Geosystems*, *17*, 1349–1369. https://doi.org/10.1002/2015GC006143

Parker, F. L. (1962). Planktonic foraminiferal species in Pacific sediments. *Micropaleontology*, *8*(2), 219–254. https://doi.org/10.2307/1484745

Penaud, A., Eynaud, F., Turon, J. L., Zaragosi, S., Marret, F., & Bourillet, J.-F. (2008). Interglacial variability (MIS 5 and MIS 7) and dinoflagellate cyst assemblages in the Bay of Biscay (North Atlantic). *Marine Micropaleontology*, *68*(1-2), 136–155. https://doi.org/10.1016/j.marmicro.2008.01.007

Pérez-Mejías, C., Moreno, A., Sancho, C., Bartolomé, M., Stoll, H., Cacho, I., et al. (2017). Abrupt climate changes during termination III in southern Europe. *PNAS*, *114*(38), 10,047–10,052. https://doi.org/10.1073/pnas.1619615114

Pflaumann, U., Duprat, J., Pujol, C., & Labeyrie, L. D. (1996). SIMMAX: A modern analog technique to deduce Atlantic sea surface temperatures from planktonic foraminifera in deep-sea sediments. *Paleoceanography*, *11*(1), 15–35. https://doi.org/10.1029/95PA01743

Pisias, N. G., & Mix, A. C. (1988). Aliasing of the geologic record and the search for long-period Milankovitch cycles. *Paleoceanography*, *3*(5), 613–619. https://doi.org/10.1029/PA003i005p00613

Pracht, H., Metcalfe, B., & Peeters, F. J. C. (2018). Oxygen isotope composition of final chamber of planktic foraminifera provides evidence for vertical migration and depth integrated growth. *Biogeosciences*, *16*(2), 643–661.

Renssen, H., & Isarin, R. F. B. (2001). The two major warming phases of the last deglaciation at ~14.7 and ~11.5 ka cal BP in Europe: Climate reconstructions and AGCM experiments. *Global and Planetary Change*, *30*(1-2), 117–153. https://doi.org/10.1016/S0921-8181(01)00082-0

Roche, D., Paillard, D., & Cortijo, E. (2004). Constraints on the duration and freshwater release of Heinrich event 4 through isotope modelling. *Nature*, *432*(7015), 379–382. https://doi.org/10.1038/nature03059

Roche, D. M., Waelbroeck, C., Metcalfe, B., & Caley, T. (2018). FAME (v1.0): A simple module to simulate the effect of planktonic foraminifer species-specific habitat on their oxygen isotopic content. *Geoscientific Model Development*, *11*, 3587–3603.

Roucoux, K. H., Tzedakis, P. C., De Abreu, L., & Shackleton, N. J. (2006). Climate and vegetation changes 180,000 to 345,000 years ago recorded in a deep-sea core off Portugal. *Earth and Planetary Science Letters*, *249*(3-4), 307–325. https://doi.org/10.1016/j.epsl.2006.07.005

Ruddiman, W. F., & McIntyre, A. (1981). The North Atlantic Ocean during the last deglaciation. *Palaeogeography, Palaeoclimatology, Palaeoecology*, *35*, 145–214.

Schiebel, R., Spielhagen, R. F., Garnier, J., Hagemann, J., Howa, H., Jentzen, A., et al. (2017). Modern planktic foraminifers in the high-latitude ocean. *Marine Micropaleontology*, *136*, 1–13. https://doi.org/10.1016/j.marmicro.2017.08.004

Scussolini, P., & Peeters, F. J. C. (2013). A record of the last 460 thousand years of upper ocean stratification from the central Walvis ridge, South Atlantic. *Paleoceanography*, *28*, 426–439. https://doi.org/10.1002/palo.20041

Scussolini, P., van Sebille, E., & Durgadoo, J. V. (2013). Paleo Agulhas rings enter the subtropical gyre during the penultimate deglaciation. *Climate of the Past*, *9*(6), 2631–2639. https://doi.org/10.5194/cp-9-2631-2013

Spielhagen, R. F., & Erlenkeuser, H. (1994). Stable oxygen and carbon isotopes in planktic foraminifers from Arctic Ocean surface sediments: Reflection of the low salinity surface water layer. *Marine Geology*, *119*(3–4), 227–250. https://doi.org/10.1016/0025-3227(94)90183-X

Spindler, M., & Dieckmann, G. S. (1986). Distribution and abundance of the planktic foraminifer *Neogloboquadrina pachyderma* in sea ice of the Weddell Sea (Antarctica). *Polar Biology*, *5*(3), 185–191. https://doi.org/10.1007/BF00441699

Spindler, M., Hemleben, C., Bayer, U., Bé, A. W. H., & Anderson, O. R. (1979). Lunar periodicity of reproduction in the planktonic foraminifer *Hastigerina pelagica*. *Marine Ecology Progress Series*, *1*, 61–64. https://doi.org/10.3354/meps001061

Srinivasan, M. S., & Kennett, J. P. (1974). Secondary calcification of the planktonic foraminifer *Neogloboquadrina pachyderma* as a climatic index. *Science*, *186*(4164), 630–632. https://doi.org/10.1126/science.186.4164.630

Sverdrup, H. U. (1953). On conditions for the vernal blooming of phytoplankton. *Journal du Conseil Conseil Permanent INternational pour l'Exploration de la Mer*, *18*(3), 287–295. https://doi.org/10.1093/icesjms/18.3.287

Sverdrup, H. U., Johnson, M. W., & Fleming, R. H. (1942). *The Oceans Their Physics, Chemistry and General Biology*. Englewood Cliffs, NJ: Prentice-Hall Inc.

Tolderlund, D. S., & Bé, A. W. H. (1971). Seasonal distribution of planktonic foraminifera in the western North Atlantic. *Micropaleontology*, *17*(3), 297–329. https://doi.org/10.2307/1485143

Troelstra, S. R., Ganssen, G. M., Sennema, E. J., Klaver, G. T., Anderliesten, C., Van den Borg, K., & de Jong, A. M. F. (1987). Late Quarternary stratigraphy and sedimentology of the central North Atlantic: A progress report. *Nuclear Instruments and Methods in Physics Research*, *B29*, 317–321.

Ufkes, E., Fred Jansen, J. H., & Brummer, G.-J. A. (1998). Living planktonic foraminifera in the eastern South Atlantic during spring: Indicators of water masses, upwelling and the Congo (Zaire) river plume. *Marine Micropaleontology*, *33*(1-2), 27–53. https://doi.org/10.1016/S0377-8398(97)00032-7

Ufkes, E., & Zachariasse, W.-J. (1993). Origin of coiling differences in living *Neogloboquadrinids* in the Walvis Bay region, off Namibia, Southwest Africa. *Micropaleontology*, *39*(3), 283–287. https://doi.org/10.2307/1485901

van Kreveld, S. A., Ganssen, G. M., van Hinte, J. E., Melkert, M. M., Troelstra, S. R., van der Borg, K., & de Jong, A. M. F. (1996). A method for quantifying deep-sea carbonate dissolution using ^{14}C dating. Paper presented at the Proceedings of the 15th International 14C Conference.

Venz, K. A., Hodell, D. A., Stanton, C., & Warnke, D. A. (1999). A 1.0 Myr record of glacial North Atlantic intermediate water variability from ODP site 982 in the Northeast Atlantic. *Paleoceanography*, *14*(1), 42–52. https://doi.org/10.1029/1998PA900013

Wefer, G., Berger, W. H., Bickert, T., Donner, B., Fischer, G., Kemle-von Mücke, S., G. Meinecke, et al. (1996). Late Quaternary surface circulation of the South Atlantic: The stable isotope record and implications for heat transport and productivity. In G. Wefer, W. H. Berger, G. Siedler, & D. Webb (Eds.), *The South Atlantic: Present and Past Circulation* (pp. 461-502). Berlin: Springer.

Wit, J. C., Reichart, G. J., & Ganssen, G. M. (2013). Unmixing of stable isotope signals using single specimen $\delta^{18}O$ analyses. *Geochemistry, Geophysics, Geosystems*, *14*, 1312–1320. https://doi.org/10.1002/ggge.20101

Wit, J. C., Reichart, G.-J., Jung, S. J. A., & Kroon, D. (2010). Approaches to unravel seasonality in sea surface temperatures using paired single-specimen foraminiferal $\delta^{18}O$ and Mg/Ca analyses. *Paleoceanography*, *25*, PA4220. https://doi.org/10.1029/2009PA001857

Wolfteich, C. M. (1994). Satellite-derived sea surface temperature, mesoscale variability, and foraminiferal production in the North Atlantic. M.Sc., Massachusetts Institute of Technology/Woodshole Oceanographic Institution (80pp.). https://doi.org/10.1575/1912/5556

Wunsch, C. (2000). On sharp spectral lines in the climate record and the millennial peak. *Paleoceanography*, *15*(4), 417–424. https://doi.org/10.1029/1999PA000468

Wunsch, C., & Gunn, D. E. (2003). A densely sampled core and climate variable aliasing. *Geo-Marine Letters*, *23*(1), 64–71. https://doi.org/10.1007/s00367-003-0125-2

Zobel, B. (1973). Biostratigraphische untersuchungen an Sedimenten des Indisch-Pakistanischen Kontinentalrandes (Arabisches Meer). In "Meteor" Forsch. Ergebnisse (pp. 9–73). Berlin, Stuttgart.